Deep-Sea Research Part I 151 (2019) 103059

Contents lists available at ScienceDirect

Deep-Sea Research Part I

journal homepage: www.elsevier.com/locate/dsri

# Phytoplankton community structure in contrasting ecosystems of the Southern Ocean: South Georgia, South Orkneys and western Antarctic Peninsula

Sdena Nunes[a,*], Mikel Latasa[b], Maximino Delgado[a], Mikhail Emelianov[a], Rafel Simó[a], Marta Estrada[a,**]

[a] Institut de Ciències del Mar, CSIC, Pg. Marítim de la Barceloneta, 37-49, 08003, Barcelona, Catalunya, Spain
[b] Centro Oceanográfico de Gijón/Xixón (IEO), Avda. Príncipe de Asturias 70bis, 33212, Gijón/Xixón, Asturias, Spain

ARTICLE INFO

*Keywords:*
Southern ocean
Phytoplankton distribution
Microscopy
HPLC
CHEMTAX
Pigments
Dimethylated sulfur

ABSTRACT

The relationships between taxonomy and distribution of the phytoplankton and environmental parameters were studied in four contrasting zones (North of the South Orkney Islands = NSO, Southeast of the South Orkney Islands = SSO, Northwest of South Georgia = NSG and West of Anvers = WA) of the Atlantic sector of the Southern Ocean, during the PEGASO cruise of the BIO Hespérides (January–February 2015). The structure of the phytoplankton community was determined by microscopic examination and by pigment analyses using high-performance liquid chromatography (HPLC) followed by application of the CHEMTAX algorithm. Overall, a statistically significant association was found between fluorometric and HPLC determinations of chlorophyll *a*, and between chemotaxonomic and microscopy-derived estimates of the contribution of diatoms, dinoflagellates and cryptophytes, although cryptophytes appeared to be underestimated by the microscopic observations. The highest average levels of fluorometric chlorophyll *a* (517 mg $m^{-2}$) were found at NSG, followed by WA (132 mg $m^{-2}$), NSO (120 mg $m^{-2}$) and SSO (34 mg $m^{-2}$). The phytoplankton community at NSG was dominated by diatoms like *Eucampia antarctica* and *Thalassiosira* spp. Cryptophytes and diatoms (mainly *Corethron pennatum*, small *Thalassiosira* spp. and *Fragilariopsis* spp.) were the most abundant chemotaxonomic groups at NSO, followed by haptophytes types 6 + 7, *Phaeocystis*-like (haptophytes type 8) and, especially in the deeper levels of the euphotic zone, pelagophytes. At SSO, the most important groups were haptophytes types 6 + 7, followed by diatoms (with a combination of taxa similar to that of NSO), *Phaeocystis*-like and pelagophytes. The main CHEMTAX groups at WA were cryptophytes (between surface and about 40 m depth), haptophytes types 6 + 7 and diatoms. The ratio between the photoprotective pigment diadinoxanthin and the sum of the light harvesting pigments of diadinoxanthin-containing phytoplankton (sum of 19′-butanoyloxyfucoxanthin, 19′-hexanoyloxyfucoxanthin, fucoxanthin and peridinin) was highest at SSO, indicating exposure to a high irradiance environment, and presented a significant positive correlation with the euphotic zone depth. The ratios of the algal osmolyte dimethylsulfoniopropionate and the trace gas dimethylsulfide to chlorophyll *a* showed the same pattern across zones, highlighting the role of light-related ecophysiology in combination with taxonomy in regulating the production of dimethylated sulfur by plankton communities.

## 1. Introduction

The Southern Ocean (SO) plays a substantial role in regulating and controlling the climate in the world. One of its main features is the Antarctic Circumpolar Current (ACC), which flows clockwise around Antarctica, connecting the Atlantic, Indian and Pacific oceans. The SO covers about 30% of the global ocean and large parts of it are high-nutrient low-chlorophyll (HNLC) areas, mainly due to the co-limitation of light and micronutrients such as iron. Despite widespread limitation to productivity, it is a large sink for anthropogenic $CO_2$ in the world and accounts for about 43% of the ocean uptake of anthropogenic $CO_2$ released to the atmosphere over the historical period (Frölicher et al.,

* Corresponding author.
** Corresponding author.
*E-mail addresses:* sdena@icm.csic.es (S. Nunes), mikel.latasa@ieo.es (M. Latasa), mdelgadom9@hotmail.com (M. Delgado), mikhail@icm.csic.es (M. Emelianov), rsimo@icm.csic.es (R. Simó), marta@icm.csic.es (M. Estrada).

https://doi.org/10.1016/j.dsr.2019.06.005
Received 29 May 2018; Received in revised form 31 May 2019; Accepted 7 June 2019
Available online 24 June 2019

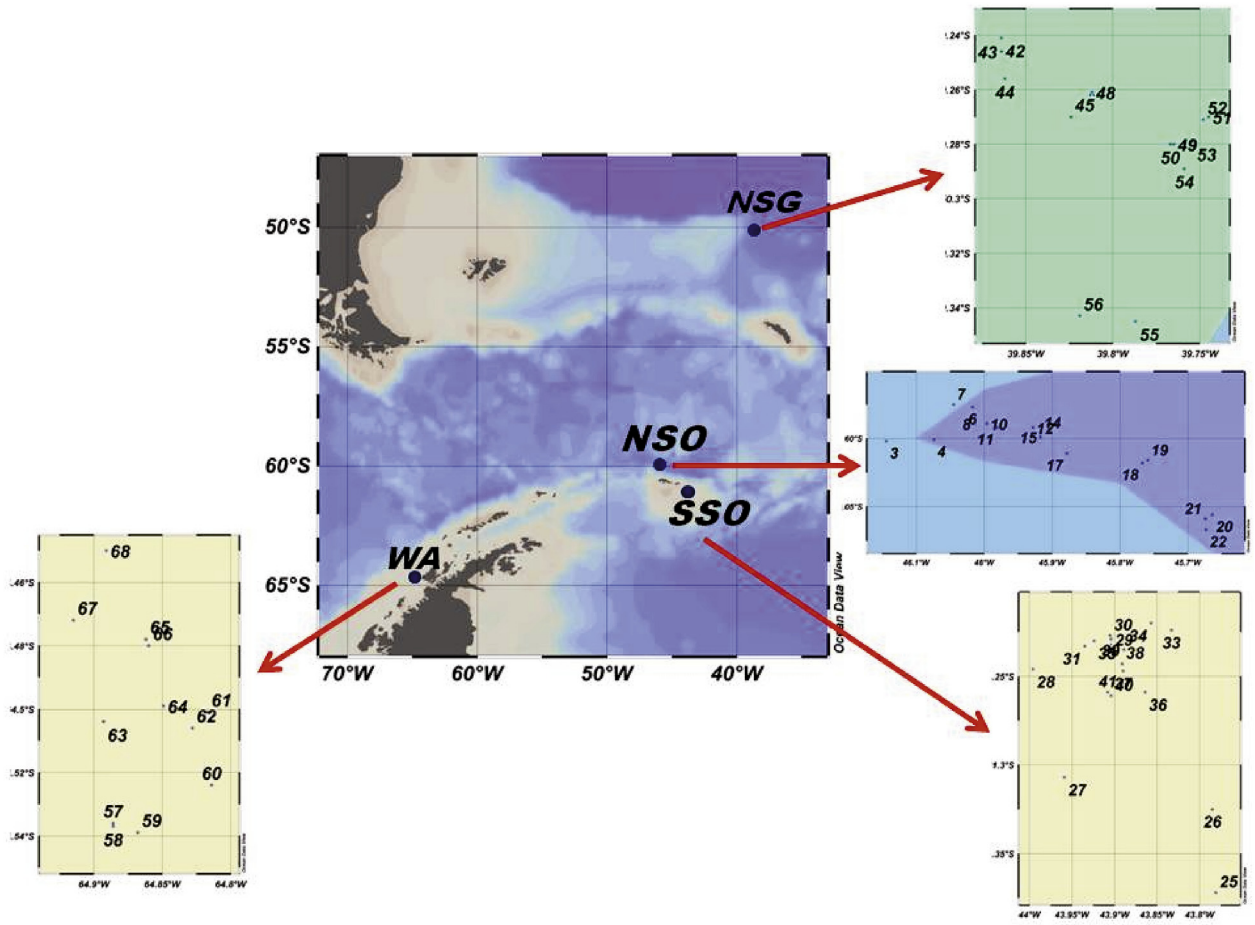


**Fig. 1.** Position of the sampling stations in the four visited zones: NSO = North of the South Orkney Islands, SSO = South of the South Orkney Islands, NSG = Northwest of South Georgia Island, WA = West of Anvers Island.

2015). This control occurs mainly through $CO_2$ solubility in the water and by action of the so-called biological pump – $CO_2$ capture by phytoplankton photosynthesis in surface waters of localized high-productivity areas, vertical transport of organic matter and carbon sequestration in the deep ocean and the sediment (Boyd and Trull, 2007; Marinov et al., 2008). Besides contributing to ocean carbon sequestration, phytoplankton plays a key role in the metabolism of sulfur compounds and may contribute to the formation of organic aerosols. In particular, some phytoplankton groups, such as haptophytes and dinoflagellates, synthesize substantial quantities of dimethylsulfoniopropionate (DMSP), which by enzymatic action can form dimethylsulfide (DMS). These and other biogenic organic emissions can influence the optical properties of the atmosphere and the Earth radiative budget (Charlson et al., 1987; Simó, 2001).

The SO contains very diverse environments, which influence the function and structure of the corresponding phytoplankton communities. One of the key factors appears to be the availability of iron. Open waters of the ACC are generally iron-limited, while coastal regions influenced by terrestrial sources, such as areas neighboring subantarctic islands or the Antarctic Peninsula, may have adequate iron supply (Martin et al., 1990; Moore et al., 2013). Another major abiotic factor influencing phytoplankton growth in the SO is light availability and its interaction with water column mixing, in turn affected by wind forcing and stabilization associated with ice melt (Vernet et al., 2008; Cassar et al., 2011).

Phytoplankton blooms in the Atlantic sector of the SO tend to be dominated by diatoms or haptophytes like *Phaeocystis* spp. (Estrada and Delgado, 1990; Mendes et al., 2013) but cryptophyte proliferations may also be important, in particular in areas influenced by melting ice (Schloss and Estrada, 1994; Moline et al., 2004). Documenting the composition of the phytoplankton communities is important for understanding food web dynamics, biogeochemical cycling and aerosol production, and for projecting potential responses of the ecosystem to climate change.

The PEGASO oceanographic cruise, on board the RV Hespérides was conducted in the Atlantic sector of the SO as part of the PEGASO project, which investigated the role of planktonic community structure, activity and physiological state, in parallel to measurements of aerosol chemistry and physics. The survey included series of oceanographic stations in four contrasting zones (or sub-regions) of the SO, located in the vicinity of the South Orkneys, the South Georgia and the Anvers Islands. The reasoning for selecting these zones was a combination of differences in hydrographic conditions, nutrient availability (in particular with respect to iron) and relatively slow currents without stable direction. A Lagrangian approach using drifters or icebergs as markers was applied within each zone to locate the stations and a suite of physical, chemical and biological measurements was conducted at each of them. Within this context, the present work deals with the quantitative distribution and taxonomic composition of the phytoplankton communities. Previous phytoplankton work in or near our study zones had been based either on microscopy (Priddle et al., 1986; Atkinson et al., 2001; Ward et al., 2008; Garibotti et al., 2005; Luan et al., 2013) or on High Performance Liquid Chromatography (HPLC) determinations (Moline et al., 1997; Gibberd et al., 2013), with only few studies combining both approaches (Rodríguez et al., 2002; Garibotti et al., 2003; Mendes et al., 2015). We used HPLC analysis of phytoplankton pigments (Roy et al., 2011), followed by application of the CHEMTAX algorithm (Mackey et al., 1996) to estimate the quantitative

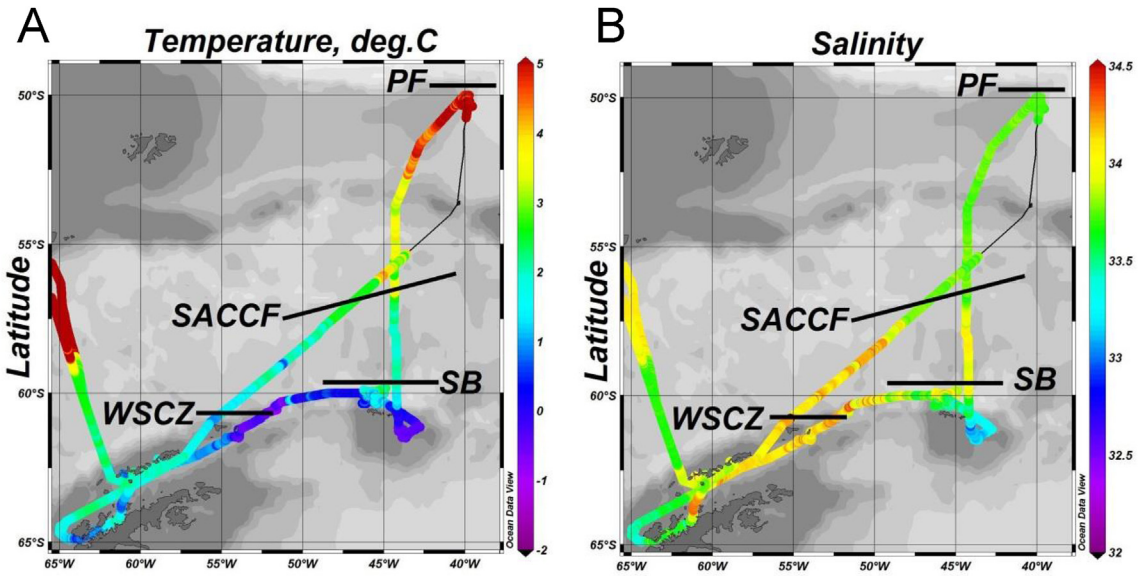


**Fig. 2.** Track of the research vessel, with sea surface temperatures (A) and salinity (B), recorded with a flow-through termosalinograph, coded in color. The position of the main oceanic fronts across the track is indicated: Polar Front (PF; 50°S), Southern Antarctic Circumpolar Current Front (SACCF,56.8°S-57.2°S), Southern Boundary of the Antarctic Circumpolar Current (SB; 59.9°S), and Weddell Scotia Confluence Zone (WSCZ; 60.0°S-60.8°S). Figure produced with the Ocean Data View software (Schlitzer, 2016). (For interpretation of the references to color in this figure legend, the reader is referred to the Web version of this article.)

contribution of major phytoplankton groups (including pelagophytes, which had not been previously assessed in the region) to total chlorophyll a (Chl *a*) and we combined these results with microscopic observations of nano- and microphytoplankton to refine the identification of the main nano- and microphytoplankton taxa. The specific aims of this study were to compare the results obtained by means of microscopy and HPLC, to use pigment composition to assess physiological variability at diel scales under contrasting ecological conditions and to document the links between phytoplankton community structure and environmental drivers and properties.

## 2. Material and methods

### 2.1. PEGASO study location and sampling

This survey was conducted on board the B.I.O. Hespérides in the austral summer of 2015 (From January, 02 to February, 12). Four zones or sub-regions (Fig. 1) were chosen for a several-day study following a Lagrangian approach: north of the South Orkney Islands (NSO), southeast of the South Orkney Islands (SSO), northwest of South Georgia (NSG) and west of Anvers (WA). The position of the main hydrographic fronts during the cruise (Figs. 2 and S1A) was determined, following the scheme of Orsi et al. (1995), with reference to the continuous records of temperature and salinity (thermosalinograph SBE 21 SeaCAT), current velocity and direction measured with the Shipboard Acoustic Doppler Current Profiler (SADCP) "Ocean Surveyor" at 75 khz, and the synoptic modeling data obtained from the Global Real-Time Ocean Forecast System (Global RTOFS) (Dall'Osto et al., 2017). We also consulted 8-day average satellite images of chlorophyll *a* concentration and sea surface temperature obtained from the Visible and Infrared Scanner (VIRS), NASA. We did not measure micronutrients, but evidence from prior studies places NSG as iron-sufficient and considers open sea areas of the ACC as HNLC regions due to iron limitation (Martin et al., 1990; Nielsdóttir et al., 2012). In three of the zones (NSO, NSG and WA), the studied water bodies were marked by means of WOCE (World Ocean Circulation Experiment) standard drifters provided with Iridium communication system; in SSO, icebergs were used as Lagrangian "markers" (see Fig. 2).

Conductivity-temperature-depth (CTD) data were obtained with a SeaBird 911 Plus multi-parametric probe and underway measurements of temperature and conductivity (salinity) were performed with a thermosalinograph (TSG) SBE21. All SBE sensors were calibrated by Sea-Bird Scientific manufacturer according their protocols (https://www.seabird.com/service-calibration-information). For data quality control, a double set of temperature and conductivity sensors was installed on the CTD probe, and the differences between temperature and conductivity (salinity) data, obtained by at the same time by each pair of temperature or salinity sensors were analyzed during the raw data conversion. Further data processing was performed with Sea-Bird software, following the recommendations of the manufacturer https://www.seabird.com/software. The quality control of underway TSG measurements was performed by periodical sampling of the water input and further salinity analysis on board by means of a Guildline 8410-A Portasal salinometer (http://www.guildline.com/).

CTD casts using the SBE 911 Plus sonde attached to a rosette of 24 12-L PVC Niskin bottles were carried out at least once a day, around 8:30 solar (local) time. In addition, a 36-h cycle was sampled in each zone, with CTD casts every 4 h starting generally at 9:30 and ending at 17:00 (solar times) the day after (see Table S1 for station information). Solar time calculations were performed by means of the NASA Solar Calculator (https://www.esrl.noaa.gov/gmd/grad/solcalc/, accessed on 15 December 2017). Conductivity, temperature, depth, *in vivo* fluorescence (with a WET Labs ECO-AFL/FL fluorometer) and photosynthetically active radiation (PAR, measured with a LI-COR Biospherical PAR Sensor) profiles were recorded down to 400 m. Water samples were taken from the Niskin bottles, at six different depths. Generally, these included "surface" (4 m depth), a "deep" level ranging between 120 m and 150 m, and four additional levels in between (Table S1). Fluorometric Chl *a* (Fl_Chl *a*) determination and phytoplankton pigment analyses were carried out for all six depths. Major nutrients, DMS and DMSP were analyzed for surface samples. Water samples for phytoplankton identification by microscopy were collected from surface and the depth of maximum fluorescence, generally the 1% light depth. Mixed layer depth was estimated in as the first depth for which water density was 0.125 kg $m^{-3}$ higher than at surface (Monterey and Levitus, 1997).

**Table 1**
Range (minimum: Min and maximum: Max), mean and standard deviation (SD) of integrated values (in mg $m^{-2}$) between 0 and 100 m depth of the main phytoplankton pigments and of T_Chl *a* for the study zones. Sub-regions are (See Fig. 1): NSO = North of the South Orkney Islands, SSO = South of the South Orkney Islands, NSG = Northwest of South Georgia Island, WA = West of Anvers Island.

| Pigment name | Abbreviation | NSO region | | | | SSO region | | | |
|---|---|---|---|---|---|---|---|---|---|
| | | Min | Max | Mean | SD | Min | Max | Mean | SD |
| 19′-butanoyloxyfucoxanthin | 19-But | 6.96 | 10.50 | 8.40 | 1.15 | 1.24 | 4.25 | 2.27 | 0.92 |
| 19′-hexanoyloxyfucoxanthin | 19-Hex | 5.82 | 9.82 | 7.36 | 1.39 | 3.83 | 8.32 | 6.11 | 1.40 |
| α-carotene | α-Car | 0.40 | 0.72 | 0.52 | 0.09 | 0.03 | 0.16 | 0.10 | 0.04 |
| β-carotene | β-Car | 0.98 | 2.08 | 1.48 | 0.30 | 0.27 | 0.83 | 0.44 | 0.16 |
| Alloxanthin | Allo | 3.15 | 6.02 | 4.76 | 0.72 | 0.22 | 0.50 | 0.40 | 0.09 |
| Diadinoxanthin | Ddx | 4.59 | 6.28 | 5.30 | 0.54 | 1.49 | 3.70 | 2.68 | 0.65 |
| Fucoxanthin | Fuco | 17.32 | 24.66 | 19.70 | 1.95 | 2.76 | 14.74 | 5.62 | 3.97 |
| Lutein | Lut | 0.24 | 1.63 | 0.59 | 0.38 | 0.05 | 0.30 | 0.13 | 0.08 |
| Peridinin | Per | 0.92 | 1.97 | 1.34 | 0.38 | 0.30 | 0.83 | 0.49 | 0.17 |
| Prasinoxanthin | Pras | 0.18 | 0.45 | 0.27 | 0.07 | 0.09 | 0.60 | 0.34 | 0.15 |
| Violaxanthin | Viol | 0.33 | 1.74 | 0.54 | 0.37 | 0.05 | 0.64 | 0.21 | 0.18 |
| Zeaxanthin | Zea | 0.56 | 1.23 | 0.84 | 0.16 | 0.20 | 0.61 | 0.37 | 0.11 |
| Chlorophyll *b* | Chl *b* | 3.01 | 4.84 | 4.08 | 0.46 | 0.41 | 6.96 | 2.45 | 1.94 |
| Chlorophyll *c2* | Chl $c_2$ | 7.57 | 15.80 | 10.77 | 2.36 | 1.64 | 7.22 | 3.25 | 1.78 |
| Chlorophyll *c3* | Chl $c_3$ | 2.98 | 7.53 | 4.84 | 1.37 | 1.07 | 4.91 | 2.32 | 1.28 |
| Monovinyl Chlorophyllide *a* | MV-Chlide *a* | 0.32 | 3.40 | 1.52 | 1.20 | 0.55 | 2.03 | 1.11 | 0.49 |
| Monovinyl chlorophyll *a* allomer 1 | MV-Chl *a*-allomer1 | 0.52 | 1.03 | 0.77 | 0.13 | 0.07 | 0.37 | 0.20 | 0.10 |
| Monovinyl chlorophyll *a* allomer 2 | MV-Chl *a*-allomer2 | 0.30 | 0.55 | 0.45 | 0.07 | 0.00 | 0.21 | 0.09 | 0.07 |
| Monovinyl chlorophyll *a* | MV-Chl *a* | 51.67 | 77.67 | 61.33 | 8.33 | 10.66 | 39.96 | 18.93 | 9.25 |
| Monovinyl chlorophyll *a* epimer | MV-Chl *a*-epimer | 0.78 | 2.06 | 1.37 | 0.44 | 0.12 | 0.41 | 0.21 | 0.08 |
| Σ pheophorbide *a* | Phaeob | 6.36 | 9.65 | 7.71 | 0.92 | 1.26 | 3.84 | 2.66 | 0.84 |
| Σ phaeophytin *a* | Phaeop | 2.27 | 3.52 | 2.83 | 0.42 | 0.30 | 1.16 | 0.79 | 0.27 |
| Total chlorophyll *a* | T_Chl *a* | 56.75 | 85.5 | 67 | 9.21 | 11.6 | 43.2 | 20.8 | 9.9 |

| Pigment name | Abbreviation | NSO region | | | | SSO region | | | |
|---|---|---|---|---|---|---|---|---|---|
| | | Min | Max | Mean | SD | Min | Max | Mean | SD |
| 19′-butanoyloxyfucoxanthin | 19-But | 4.02 | 7.49 | 5.10 | 0.95 | 2.07 | 3.05 | 2.53 | 0.37 |
| 19′-hexanoyloxyfucoxanthin | 19-Hex | 9.24 | 14.65 | 10.79 | 1.93 | 5.92 | 8.13 | 6.91 | 0.86 |
| α-carotene | α-Car | 0.13 | 0.34 | 0.21 | 0.07 | 0.87 | 2.31 | 1.53 | 0.50 |
| β-carotene | β-Car | 2.26 | 7.21 | 5.11 | 1.55 | 0.80 | 1.37 | 1.00 | 0.18 |
| Alloxanthin | Allo | 0.47 | 1.18 | 0.85 | 0.25 | 7.29 | 19.87 | 13.48 | 3.55 |
| Diadinoxanthin | Ddx | 10.00 | 31.24 | 22.38 | 6.63 | 2.93 | 4.97 | 3.74 | 0.66 |
| Fucoxanthin | Fuco | 57.14 | 236 | 155 | 54.07 | 9.12 | 17.05 | 12.52 | 2.35 |
| Lutein | Lut | 0.38 | 0.52 | 0.46 | 0.05 | 0.57 | 1.24 | 0.81 | 0.23 |
| Peridinin | Per | 2.88 | 4.40 | 3.73 | 0.47 | 0.28 | 0.69 | 0.43 | 0.12 |
| Prasinoxanthin | Pras | 0.40 | 0.79 | 0.60 | 0.10 | 0.35 | 0.55 | 0.42 | 0.06 |
| Violaxanthin | Viol | 0.13 | 0.49 | 0.22 | 0.10 | 0.09 | 0.14 | 0.11 | 0.02 |
| Zeaxanthin | Zea | 2.44 | 6.39 | 4.27 | 1.18 | 0.41 | 0.80 | 0.60 | 0.14 |
| Chlorophyll *b* | Chl *b* | 1.13 | 2.32 | 1.62 | 0.40 | 1.02 | 1.47 | 1.18 | 0.13 |
| Chlorophyll *c2* | Chl $c_2$ | 25.06 | 89.54 | 58.69 | 17.94 | 8.08 | 17.29 | 11.17 | 2.94 |
| Chlorophyll *c3* | Chl $c_3$ | 11.29 | 36.09 | 24.38 | 6.96 | 2.80 | 6.71 | 4.42 | 1.32 |
| Monovinyl Chlorophyllide *a* | MV-Chlide *a* | 1.04 | 13.66 | 3.19 | 3.53 | 0.37 | 0.75 | 0.48 | 0.12 |
| Monovinyl chlorophyll *a* allomer 1 | MV-Chl *a*-allomer1 | 1.42 | 4.61 | 2.70 | 1.00 | 0.45 | 1.21 | 0.83 | 0.29 |
| Monovinyl chlorophyll *a* allomer 2 | MV-Chl *a*-allomer2 | 0.85 | 2.83 | 1.92 | 0.57 | 0.24 | 0.45 | 0.35 | 0.07 |
| Monovinyl chlorophyll *a* | MV-Chl *a* | 123 | 374 | 254 | 73.9 | 31.73 | 78.15 | 52.63 | 13.78 |
| Monovinyl chlorophyll *a* epimer | MV-Chl *a*-epimer | 3.85 | 7.82 | 5.64 | 1.34 | 0.23 | 1.08 | 0.83 | 0.25 |
| Σ phaeophorbide *a* | Phaeob | 35.75 | 81.22 | 59.30 | 11.43 | 6.60 | 8.69 | 7.42 | 0.65 |
| Σ phaeophytin *a* | Phaeop | 9.08 | 21.87 | 16.41 | 4.35 | 1.34 | 2.41 | 1.87 | 0.35 |
| Total chlorophyll *a* | T_Chl *a* | 135 | 408 | 282 | 80.9 | 37.2 | 85.9 | 60 | 14.5 |

### *2.2. Nutrient concentration, fluorometric Chl a (Fl_Chl a) and DMS and DMSP determinations*

Water for nutrient analyses was placed (without previous filtration) in Falcon vials and kept frozen at −20 °C until processing in the land laboratory. Phosphate, nitrate, nitrite and silicate concentrations were determined with a Bran+Luebbe AA3 AutoAnalyzer, following the procedures of Hansen and Koroleff (1999).

For Fl_Chl *a* determination, 100 $cm^3$ of water were filtered through Whatman GF/F fibre filters (25 mm diameter), which were subsequently placed in a freezer at −20 °C. After several hours, the filters were introduced in vials with 90% acetone and left in the dark at 4 °C for about 24 h. The fluorescence of the extracts was measured with a Turner Designs fluorometer according to the procedure described in Yentsch and Menzel (1963). No "phaeophytin" correction was applied.

Aqueous (GFF-filtered) concentrations of DMS were determined with a purge and trap gas chromatograph (GC) coupled to a mass spectrometry detector; total (particulate + dissolved, largely particulate) DMSP was determined by alkaline hydrolysis of unfiltered samples, analysis by purge and trap GC with flame photometric detection, subtraction of the endogenous DMS (Dall'Osto et al., 2017).

### *2.3. Phytoplankton identification*

Immediately after collection, 250 $cm^3$ of seawater were placed in amber glass flasks, preserved with formalin-hexamine solution to a final concentration of 1% formalin and stored in the dark until analysis. For phytoplankton identification 100 $cm^3$ methacrylate settling chambers were filled with the seawater sample. After 48 h of sedimentation, the chamber bottom was separated and examined under a XSB-1A inverted

microscope (Utermöhl, 1958). The entire base of the chambers was scanned at 125× to quantify the less abundant and larger organisms of the microphytoplankton (> 20 μm), and at least two transects were examined at 312× to enumerate the smaller and more abundant organisms of the nanoplankton (< 20 μm). On occasions of exceptionally high concentrations, 6 fields were counted at 312×. Phytoplankton was identified to the species level, when possible. However, many organisms could not be adequately classified and were pooled in categories such as "small dinoflagellates (< 20 μm)", "unidentified centric diatoms" or "unidentified small coccolithophores (< 10 μm)". The inverse microscope method is not adequate for the small organisms of the picoplankton. Our counts, thus, include nano- and microplankton. For the purpose of comparison with the pigment data, we classified the organisms into the following groups: dinoflagellates, diatoms, coccolithophores, cryptophytes and other. For brevity, we will refer to these groups as "phytoplankton", although many dinoflagellates are heterotrophs. For biovolume estimation, maximum and minimum length, and maximum and minimum width were recorded for each taxon, using a digital camera and the Scope Photo software after calibration for the employed microscope; average values from these measurements were used to calculate the volume of approximate geometric shapes: ellipsoid for dinoflagellates, coccolithophores and flagellates, cylinder for centric diatoms and prisma for pennate diatoms (a simplified version of the shapes proposed by Hillebrand et al., 1999). Biovolume estimates referred to the main part of the body, so that setae and other appendages were not included. The main references for taxonomical identification were Sournia (1986), Ricard (1987), Chrétiennot-Dinet (1990), Rampi and Bernard (1980), Cros and Fortuño (2002), Tomas (1993, 1995) and UNESCO (1995).

### 2.4. HPLC pigment analysis

Pigment composition was determined by HPLC (Latasa, 2014). Briefly, 0.65–1 L of seawater were filtered onto Whatman GF/F (nominal pore size 0.7 μm; 25 mm diameter) glass fiber filter under dim light. The filters were folded, introduced into cryovials and frozen at −80 °C until analysis on land, at the Centro Oceanográfico de Gijón (IEO, Instituto Español de Oceanografía, Spain). For analysis, the filters were placed in Nalgene tubes with 2.5 $cm^3$ of 90% acetone in which an internal standard of apo-8′-carotenal (Fluka) had been dissolved. The tubes were chilled in ice, sonicated during 30 s and stored for 24 h at -20 °C. Afterwards, the samples were vortexed, filtered through Whatman GF/F glass fiber filters to remove filter debris and immediately injected into the HPLC instrument [Agilent series (Waldbronn, Germany) 1200 chromatographic system with a G1311A quaternary pump, a G1367C autosampler with a 100 μL capillary loop, a G1316B column thermostat, and a G1315C diode array detector]. Sample extract/water ratios of 60/40 were used, according to Latasa (2014). Pigments (Table 1) were identified at 474 and 664 nm. The total monovinyl-chlorophyll *a* concentration (T_Chl *a*) was estimated as the sum of monovinyl-chlorophyll *a*, chlorophyllide *a*, chlorophyll *a* epimer and chlorophyll *a* allomers. No divinyl-chlorophyll *a* was detected.

### 2.5. Photoprotective pigment index

Variations in irradiance intensity may alter the concentrations and composition of phytoplankton pigments (Higgins et al., 2011). To assess the photoacclimation response of at least the part of the phytoplankton sharing diadinoxanthin as the main light-protecting pigment (which includes diatoms, dinoflagellates, haptophytes and pelagophytes), we calculated the ratio Ddx/(LHC) between the concentration of diadinoxanthin (Ddx) and the sum of the concentrations (LHC) of the main light-harvesting carotenoids: fucoxanthin (Fuco), 19′-butanoyloxyfucoxanthin (19-But), 19′-hexanoyloxyfucoxanthin (19-Hex) and peridinin (Per).

### 2.6. CHEMTAX

The relative abundance of microalgal groups contributing to total Chl *a* biomass was derived from pigment concentration data using version 1.95 of the CHEMTAX chemical taxonomy software (Mackey et al., 1996). This program uses one or several initial matrices of pigment/T_Chl *a* ratios for the selected phytoplankton groups and performs iterations to optimize the proportion of T_Chl *a* accounted for by these groups. The final result of the CHEMTAX program consists of a new adjusted matrix of pigment quotients and a list of the contribution of each pigmentary class to the concentration of each pigment. The initial pigment ratios used in this work were based on diagnostic pigments and pigment matrices used in studies from the Antarctic region (Rodríguez et al., 2002; Kozlowski et al., 2011). The pigments considered were Per, 19-But, 19-Hex, alloxanthin (Allo), chlorophyll *b* (Chl *b*), chlorophyll *c*2 (Chl *c*2), Fuco, lutein (Lut), prasinoxanthin (Pras), violaxanthin (Viol) and zeaxanthin (Zea). The haptophytes, characterized by the occurrence of 19-Hex, were divided in two groups, according to the important presence of 19-But (type 8, which comprises *Phaeocystis*) or to the negligible content of this pigment (a combination of types 6 and 7, including the coccolithophores and *Chrysochromulina*). The samples of each study sub-region were clustered according to the application of Ward's method to a similarity matrix based on Manhattan distances, using the Statistica v.5.5 software. A total of 13 clusters was identified, corresponding 3 to NSO and SSO, 5 to NSG and 2 to WA. For each cluster, we followed the procedures of Latasa (2007) and Latasa et al. (2010), i.e. we created 29 randomized copies of the initial ratio matrix and we ran the program for eight successive times. After the eighth run, a single average matrix was made and used again for a final run of each cluster (Table S2). Eight pigmentary classes were quantified: Chlorophytes, cryptophytes, diatoms, dinoflagellates, haptophytes types 6 + 7, prasinophytes, haptophytes type 8 (hereafter "*Phaeocystis*-like") and pelagophytes.

### 2.7. Statistical analyses

The relationships between the composition of the phytoplankton community (as represented by the biomass of the eight CHEMTAX-derived groups, in mg $m^{-3}$ of Chl *a*) at 4 m depth and abiotic parameters (temperature, salinity, oxygen, turbidity, transmission, nitrate, phosphate and Fl_Chl *a*) measured at the same depth plus the MLD of each station were summarized by means of a canonical correspondence analysis (CCA). CHEMTAX-derived Chl *a* values were subjected to a square root transformation to reduce the influence of biomass differences. The calculations were carried out with software package XLSTAT.

## 3. Results

### 3.1. General characterization of the study sub-regions

The surface temperature and salinity records and the position of the main hydrographic fronts during the PEGASO cruise are shown in Figs. 2 and S1A. The NSO and the NSG zones were located within meanders of the Southern Boundary of the ACC (SB) and the Polar Front (PF), respectively. SSO, some 60 nautical miles to the north of the Weddell Front, was next to the marginal ice zone of the Weddell Sea. In January 2015, the characteristic position of the Weddell Front coincided with the perimeter of the > 25% ice cover (https://seaice.uni-bremen.de/ – data not shown). WA was placed on the Southern Boundary and was influenced by relatively colder and less saline coastal waters of Anvers Island.

The vertical profiles of temperature, salinity and fluorescence during the time-series sampling and the averages of the environmental parameters for the different study zones are presented in Fig. 3 and Table 2, respectively. In NSO and SSO (Fig. 3A, B, D and E; Fig. S1B),

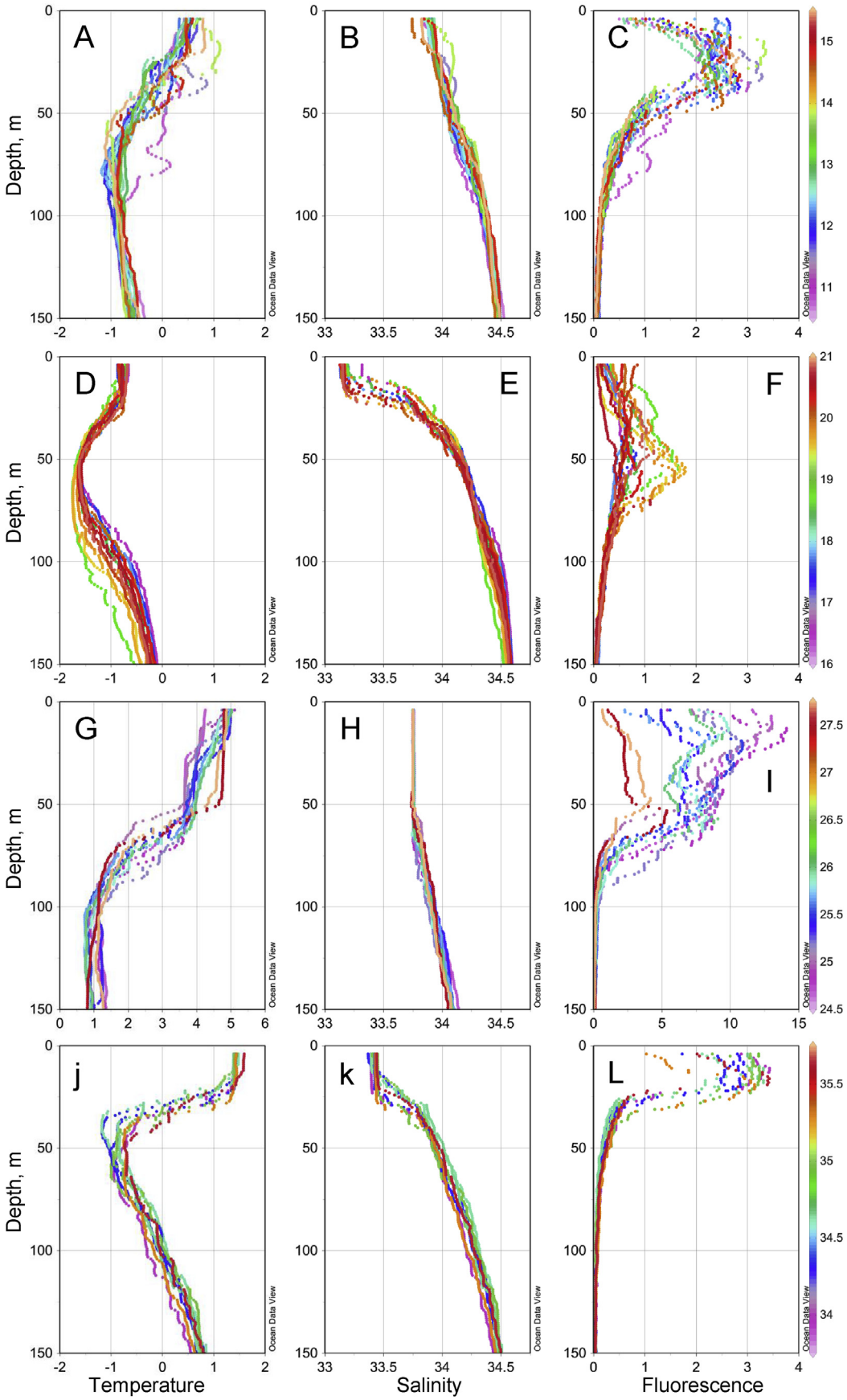


**Fig. 3.** Vertical profiles of (A, D, G, J) temperature (°C), (B, E, H, K) salinity and (C, F, I, L) fluorescence (arbitrary units) during the visits to the NSO (A, B, C), SSO (D, E, F), NSG (G, H, I) and WA (J, K, L) sub-regions. The colors represent the day of the year 2015 (color scale on the right side). See the explanation of Fig. 1 for acronyms. Figures produced with the Ocean Data View software (Schlitzer, 2016). (For interpretation of the references to color in this figure legend, the reader is referred to the Web version of this article.)

**Table 2**
Mean ± standard deviation of physico-chemical variables and ratios for the surface samples (except for Phaeo/T_Chl *a* and Ddx/LHC, which are averages for the two shallower sampling dephts), upper mixed layer depth (MLD), depth receiving 1% of surface irradiance ($Z_{1\%}$) and mean of the ratio between $Z_{1\%}$ and MLD for the stations of the studied regions (see Table 1 for sub-region acronyms). Variable abbreviations are: Fl_Chl *a* = fluorometric Chl *a*, DMSP = total (particulate + dissolved) dimethyl sulfoniopropionate, DMS = aqueous dimethyl sulfide, Phaeo = sum of phaeopigments and phaeophorbides (μg $L^{-1}$), T_Chl *a* = total Chl *a* (μg $L^{-1}$) Ddx = diadinoxanthin (μg $L^{-1}$), LHC = sum of 19-But + 19-Hex + fucoxanthin + peridinin (μg $L^{-1}$). One outlier of Phaeo/T_Chl *a* for station 45, 13 m has been excluded.

| Region | Units | NSO | | SSO | | NSG | | WA | |
|---|---|---|---|---|---|---|---|---|---|
| | | Mean | SD | Mean | SD | Mean | SD | Mean | SD |
| Temperature[a] | °C | 0.58 | 0.17 | −0.75 | 0.10 | 4.73 | 0.44 | 1.45 | 0.08 |
| Salinity[a] | | 33.84 | 0.07 | 33.16 | 0.06 | 33.74 | 0.02 | 33.41 | 0.03 |
| Oxygen[a] | μM $kg^{-1}$ | 320.3 | 1.004 | 312.4 | 0.82 | 295.6 | 7.52 | 309.3 | 1.87 |
| Turbidity[a] | NTU[b] | 0.56 | 0.01 | 0.49 | 0.003 | 0.69 | 0.06 | 0.55 | 0.01 |
| Transmission[a] | % | 84.31 | 1.09 | 92.23 | 0.30 | 83.45 | 2.98 | 77.54 | 1.84 |
| Nitrate[a] | μM | 27.31 | 1.90 | 27.55 | 3.25 | 17.17 | 1.63 | 18.71 | 0.89 |
| Nitrite[a] | μM | 0.23 | 0.06 | 0.16 | 0.02 | 0.29 | 0.04 | 0.19 | 0.03 |
| Ammonium | μM | 2.86 | 3.51 | 1.62 | 1.06 | 1.71 | 1.90 | 3.08 | 1.87 |
| Silicate[a] | μM | 47.89 | 4.07 | 47.34 | 4.65 | 2.00 | 0.39 | 49.68 | 3.66 |
| Phosphate[a] | μM | 1.99 | 0.21 | 2.14 | 0.25 | 1.29 | 0.15 | 1.79 | 0.16 |
| Fl_Chl *a*[a] | μg $L^{-1}$ | 1.87 | 0.22 | 0.32 | 0.02 | 5.05 | 0.60 | 4.05 | 0.48 |
| MLD[a] | m | 29.75 | 11.84 | 15.79 | 5.35 | 49.83 | 11.42 | 22.89 | 5.60 |
| $Z_{1\%}$ | m | 50.0 | 8.0 | 89.6 | 10.0 | 26.0 | 6.7 | 35.0 | 3.1 |
| $Z_{1\%}$/MLD | | 2.2 | 1.5 | 5.6 | 1.6 | 0.6 | 0.2 | 1.5 | 0.3 |
| DMSP | nM | 302.8 | 51.91 | 89.67 | 18.35 | 83.28 | 27.31 | 115.7 | 14.61 |
| DMS | nM | 8.19 | 1.64 | 7.88 | 1.52 | 5.97 | 1.11 | 2.13 | 0.55 |
| DMS/DMSP | | 0.03 | 0.01 | 0.09 | 0.03 | 0.08 | 0.04 | 0.02 | 0.004 |
| DMSP/Fl_Chl *a* | nmol/μg | 162.5 | 35.85 | 291.6 | 64.61 | 18.78 | 9.71 | 28.68 | 3.11 |
| DMS/Fl_Chl *a* | nmol/μg | 4.33 | 0.72 | 24.40 | 3.88 | 1.52 | 0.72 | 0.53 | 0.12 |
| Phaeo/T_Chl *a* | | 0.15 | 0.04 | 0.2 | 0.14 | 0.22 | 0.08 | 0.1 | 0.04 |
| Ddx/LHC | | 0.35 | 0.06 | 0.56 | 0.1 | 0.19 | 0.03 | 0.23 | 0.04 |

[a] Variables used in the canonical correspondence analysis.
[b] Nephelometric Turbidity Unit.

the layer of relatively cold Winter Water, centered around 70 m depth, was underlain by a relatively warm and saline Warm Deep Water derived from the Circumpolar Deep Water (CDW) of the ACC (Meredith et al., 2011) and was covered by surface layers, seasonally warmed in NSO and influenced by low salinity ice-melt water in SSO. The mean mixed layer depth (MLD) was 30 m in NSO and 16 m in SSO, where it was located just below the ice-melt surface water layer. NSG (Fig. 3G and H; Fig. S1B) was placed outside the main bloom area, which was closer to the continental shelf according to climatological data (Borrione and Schlitzer, 2013) and recent satellite images (data not shown); on the third day of the series, there was a marked change towards warmer, more saline and chlorophyll-poorer surface waters, presumably linked to movements across PF gradients; the MLD was approximately 50 m. The hydrography of the WA (Fig. 3I and J; Fig. S1B) zone is complex (Dinniman and Klinck, 2004); water masses on the shelf are episodically influenced by intrusions of Circumpolar Deep Water. During our visit, mean MLD was 23 m. Average surface nitrate and phosphate concentrations were fairly similar in all zones (the ranges were 27.6-17.2 μM for nitrate and 1.3–2.1 for phosphate, Table 2). In contrast, silicate concentration was 47–50 μM in all sub-regions except NSG, where it was around 2 μM. All zones presented subsurface fluorescence maxima (Fig. 3C, F, I and L), partly related to decreases in the *in vivo* fluorescence/Chl *a* ratio in the upper surface waters (seen also Fig. S2), as will be commented later. Average DMSP and DMS concentrations ranged respectively from 302.8 (NSO) to 83.3 (NSG) and from 8.2 (NSO) to 2.1 (WA); however, the ratios DMSP/Fl_Chl *a* and DMS/Fl_Chl *a* were highest in SSO (Table 2) and lowest in NSG and WA, respectively.

### 3.2. Phytoplankton pigments

Mean Fl_Chl a concentrations at surface (Table 2) ranged (mean ± SD) from 0.32 ± 0.06 μg $L^{-1}$ at SSO to 5.05 ± 1.98 μg $L^{-1}$ at NSG, with intermediate values for NSO (1.95 ± 0.17 μg $L^{-1}$) and WA (4.05 ± 0.48 μg $L^{-1}$). Integrated Fl_Chl *a* values (0–100 m depth) were 33.6 ± 6.2 mg $m^{-2}$ for SSO, 119.8 ± 11 mg $m^{-2}$ for NSO, 132 ± 22.6 mg $m^{-2}$ for WA and 516.8 ± 149.8 mg $m^{-2}$ for NSG. The vertical distribution of Fl_Chl *a* (Fig. S2) was fairly homogeneous throughout the mixed layer in NSO and NSG, tended to attain the highest values at surface (4 m depth) in WA and presented weak subsurface maxima below the MLD in SSO. In contrast with *in vivo* fluorescence, Fl_Chl *a* did not present surface minima. The ratio Fluo/Fl_Chl *a* between *in vivo* fluorescence (Fluo) and Fl_Chl *a* for the two upper sampling depths showed appreciable circadian variability, with lower values around noon in all sub-regions, as highlighted by significant 2-degree polynomial regressions (Fig. S3A), while for the deeper samples there were no comparable significant relationships (Fig. S3B).

The basic statistical parameters of the pigments determined by HPLC are shown in Table 1 and their average contribution, dominated by Fuco and Chl *c*2 in NSO and NSG, Fuco and 19- Hex in SSO and Fuco, 19-Hex and Allo in WA, is presented in Fig. S4. There was a good correlation between Fl_Chl *a* and T_Chl *a* as determined by HPLC (Fl_Chl *a* = 1.65 *T_Chl *a* + 0.30, n = 268, $r^2$ = 0.83, p < 0.0001) (Fig. S5), although the slope was significantly higher than 1. The ratio between the sum of phaeophorbides and phaeophytines and T_Chl *a* (Phaeo/T_Chl *a*) was calculated as an index of herbivory (Mendes et al., 2015); average values for the two shallower sampling levels of the stations of each sub-region ranged from 10% at WA to 22% at NSG (Table 2). Phaeo/T_Chl *a* was relatively homogeneous in the upper water layers but increased considerably below 50 m at NSG and WA and in the deeper samples of NSO and SSO (data not shown).

The ratio Ddx/LHC, between the concentration of the photoprotective carotenoid Ddx and the sum of the concentrations of the chromophyte light-harvesting carotenoids 19-But, 19-Hex, Fuco and Per, decreased strongly below 20–40 m depth in all sub-regions and presented the highest values in the upper mixed layer of SSO (Table 2, Figs. S6A and B). The circadian variability of Ddx/LHC in surface waters was fairly small, with slightly higher noon values in SSO and WA

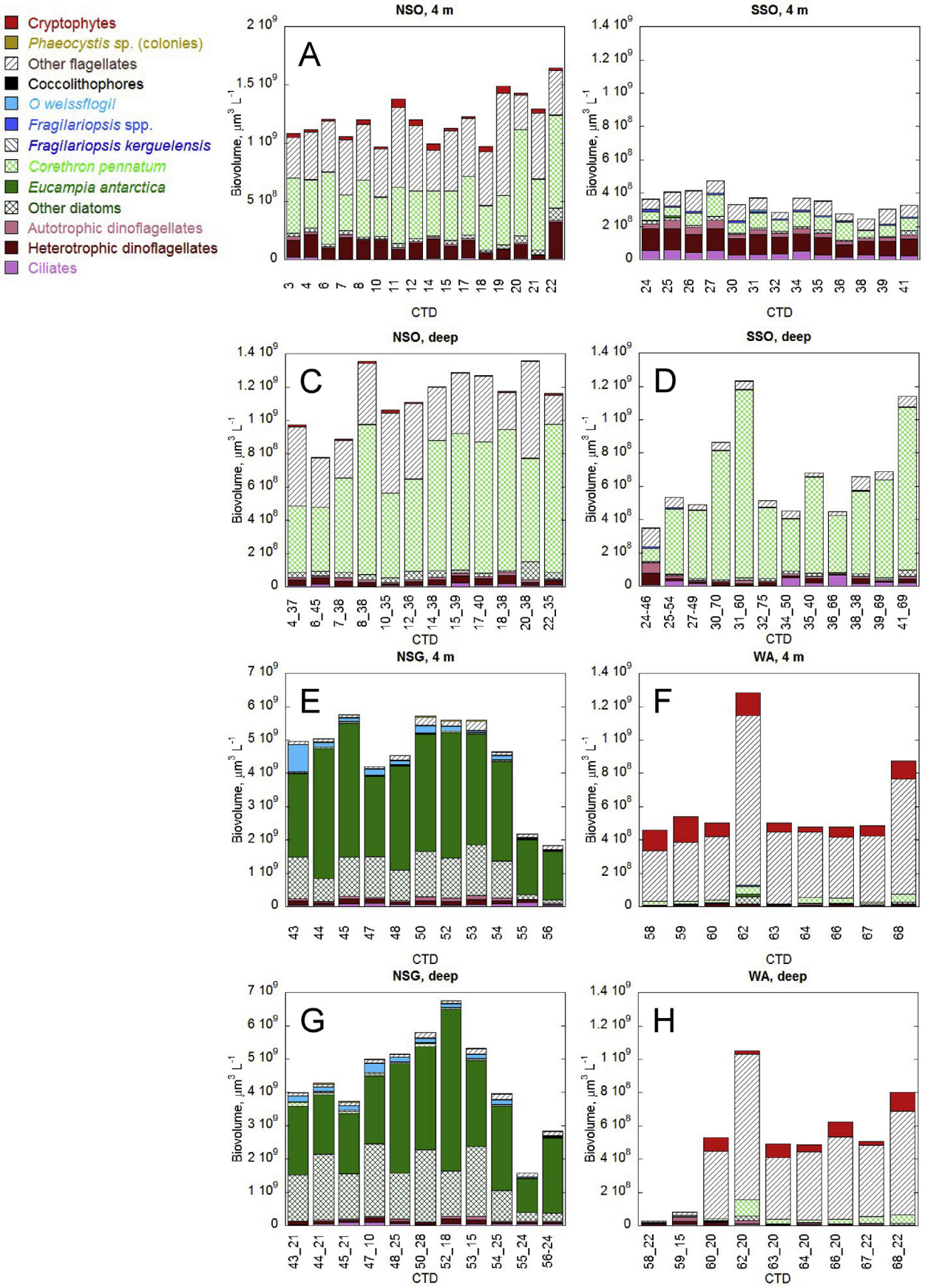


**Fig. 4.** Biovolume of selected taxa and major phytoplankton groups in the surface (4 m) and subsurface ("deep") samples taken in the four study regions. The labels of the abscissa in the "deep" samples indicate the cast number followed by the sampling depth in m. Acronyms as in Fig. 1.

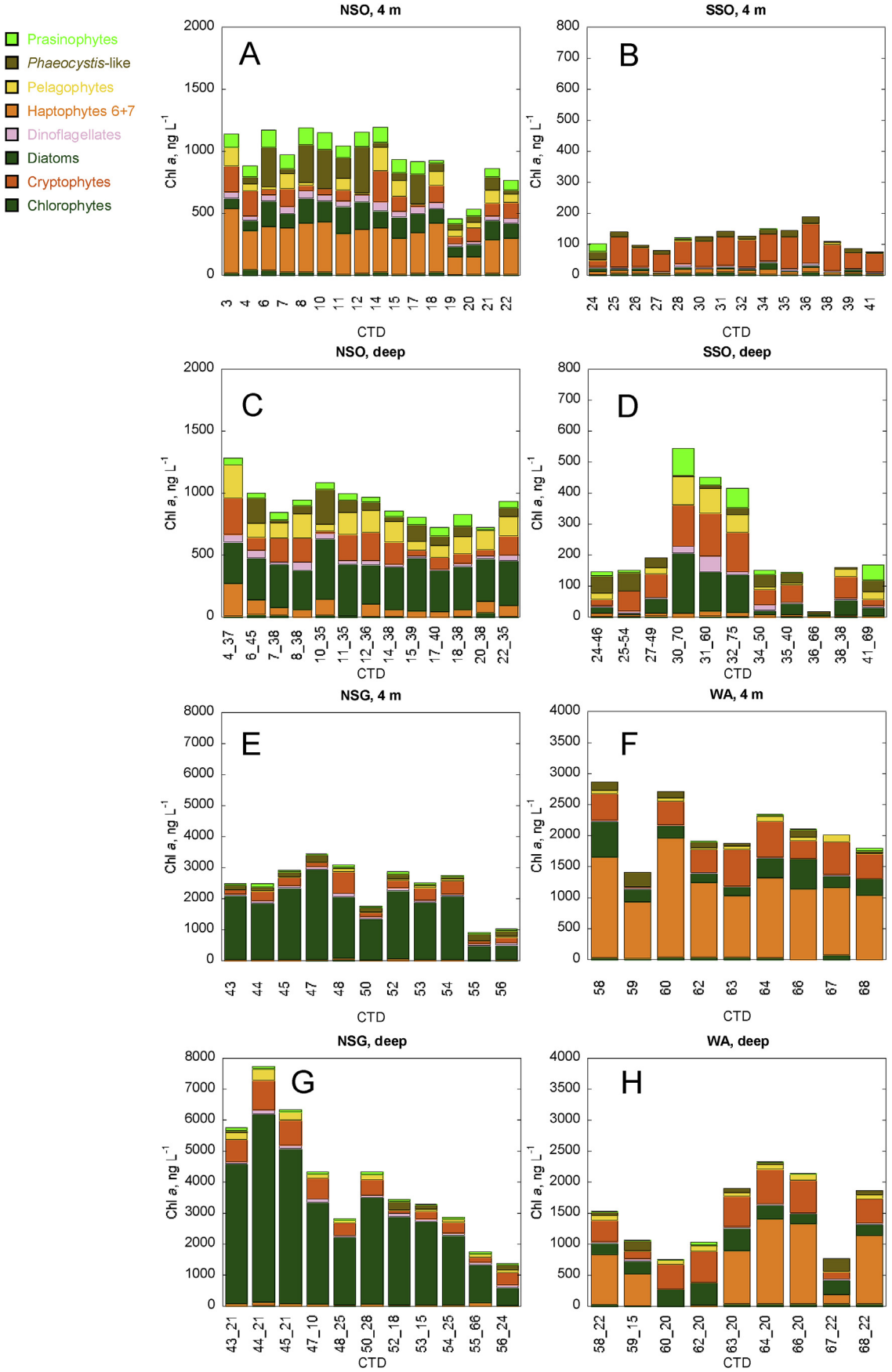


**Fig. 5.** Contribution (in ng $l^{-1}$) to total chlorophyll *a* by the CHEMTAX-derived phytoplankton groups in surface (4 m) and subsurface (deep) samples taken in the four study regions. The labels of the abscissa in the "deep" samples indicate the cast number followed by the sampling depth in m (when possible, this depth was chosen to match that of Fig. 4). Acronyms as in Fig. 1.

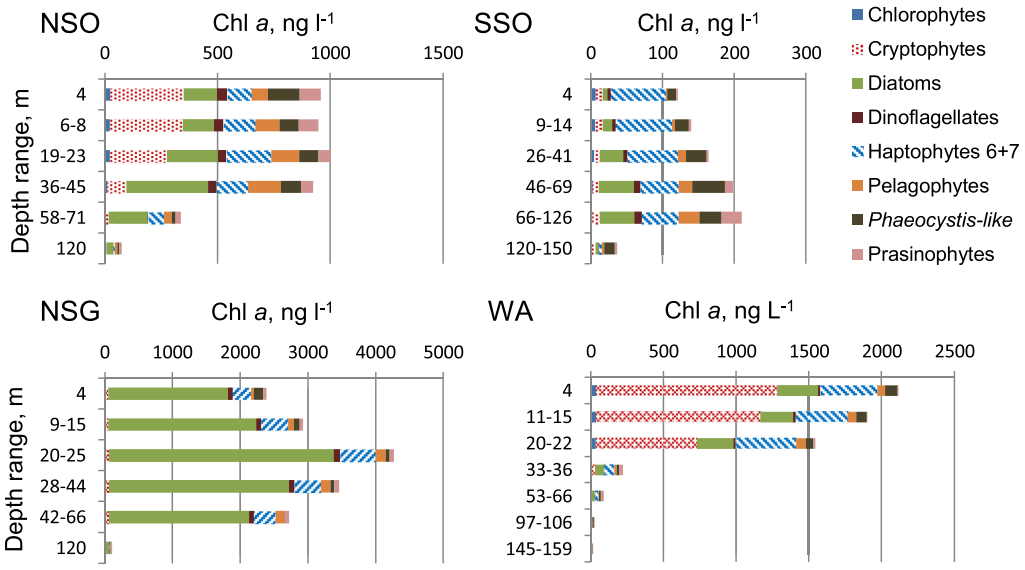


**Fig. 6.** Vertical distribution of the mean contribution to total chlorophyll a by the CHEMTAX-derived phytoplankton groups (in ng $l^{-1}$) in the four study sub-regions. Acronyms as in Fig. 1.

(Fig. S6C).

### 3.3. Phytoplankton assemblages

A total of 116 taxa, including several microzooplankton groups (such as ciliates and Radiolaria), were identified by optical microscopy in the surface and subsurface phytoplankton samples of the different stations. For each sub-region, the average abundance and biovolume of the most important taxa (in terms of biovolume) that were present in at least 25% of the samples are presented in Table S3; the biovolume contribution of some selected taxa and major groups is shown in Fig. 4. The temporal variability of the Chl *a* contribution (hereafter, referred to as Chl *a* concentration) of the eight phytoplankton groups determined by CHEMTAX is shown in Figs. 5 and S7 – S10, and the corresponding average Chl *a* concentrations for each depth is shown in Fig. 6. Comparisons between the contribution to total Chl *a* of the chemotaxonomic groups and microscopy-estimated biovolumes could be carried out for diatoms, autotrophic (and mixotrophic) dinoflagellates and cryptophytes (Fig. S11). The relationship was significant for all three groups (diatoms, $r^2 = 0.68$; autotrophic dinoflagellates, $r^2 = 0.23$; cryptophytes, $r^2 = 0.68$, $p < 0.0001$; $N = 105$, $p < 0.0001$ for all groups).

The four studied sub-regions presented marked differences in phytoplankton composition. Cryptophytes, which decreased with depth, and diatoms, which showed the opposite pattern, were the most abundant CHEMTAX groups at NSO, followed by haptophytes types 6 + 7, *Phaeocystis*-like and pelagophytes (Fig. 5A and C, Fig. 6 and Fig. S7); the most important taxa in the corresponding microscopy samples were the diatoms *Corethron pennatum*, *Thalassiosira* spp. (small) and *Fragilariopsis* spp., heterotrophic *Gyrodinium* spp. and large and small (< 20 µm) unidentified dinoflagellates, cryptophytes and nanoflagellates (Table S3, Fig. 4A and C). Haptophytes types 6 + 7, followed by diatoms and *Phaeocystis*-like, both of which increased their contribution deeper in the water column, were the most important CHEMTAX groups at SSO (Fig. 5B and D, and Fig. 6). This sub-region presented a combination of microscopy taxa similar to that of NSO (Table S3, Fig. 4B and D), but with lower *C. pennatum* and *Thalassiosira* spp. (small), higher *Fragilariopsis* spp. abundances and a smaller contribution of cryptophytes; as at NSO, diatoms were relatively more important at depth (Table S3, Figs. 4 and 5B and D, Fig. 6 and Fig. S8). NSG, the zone with highest T_Chl *a* concentration, was dominated by diatoms at all depths, both in terms of CHEMTAX-derived Chl *a* and of phytoplankton abundance and biovolume (Figs. 4 and 5 E and G, Fig. 6 and Fig. S9), but the warmer water body encountered after day 27 (Fig. 3G) was associated to a marked change in the phytoplankton composition, with lower concentrations of diatoms and increased contributions of chlorophytes and *Phaeocystis*-like (Fig. S9). The main microscopy taxa both at surface and subsurface levels (Table S3, Fig. 4E and G) were *Eucampia antarctica*, *Fragilariopsis kerguelensis*, *Thalassiosira* spp. small, *Thalassiosira* and *Porosira* spp., *Odontella weissflogii* and *Trichotoxon reinboldii*, but there was also a substantial contribution of nanoflagellates. In turn, coccolithophores were practically only present in this sub-region. The main CHEMTAX groups at WA (Fig. 5F and H, Fig. 6 and Fig. S10) were cryptophytes and haptophytes types 6 + 7 at the shallowest layers, and haptophytes, diatoms and prasinophytes at depth (below 22 m), while microscopic observations (Table S3, Fig. 4F and H) revealed cryptophytes and nanoflagellates, heterotrophic *Gyrodinium* spp., unidentified dinoflagellates and, in particular at the subsurface levels, diatoms such as *Eucampia antarctica*, *Fragilariopsis kerguelensis* and *Thalassiosira* spp. small.

The relationships between the chemotaxonomic phytoplankton groups and the physico-chemical variables and the differences among the four study zones were highlighted by the CCA, which explained 79.2% of the total variance with the two first axes. The first axis (C1) separated NSG on the negative side, from the other sub-regions. Diatoms, which characterized the NSG samples, were associated with high temperature, turbidity, MLD and Chl *a*, and low silicate, nitrate, phosphate and oxygen concentrations, whereas cryptophytes, which were particularly abundant at NSO and WA, appeared on the positive side of C1. The second CCA axis (C2) was mainly related to the variability of nitrate, oxygen and salinity and distinguished the sample clusters from NSO, SSO and WA. This axis depicted a sequence from haptophytes, associated with SSO on the positive, low salinity part of C2, to prasinophytes, which were particularly important in NSO, on the opposite part. The other groups were distributed within intermediate values of C1 and C2.

## 4. Discussion

### 4.1. Microscope-vs pigment-based quantification of phytoplankton taxa

Microscopic observations and the HPLC analysis of biomarker pigments followed by the CHEMTAX algorithm have been successfully used in many phytoplankton studies, either separately or complementing each other (Rodríguez et al., 2002; Kozlowski et al., 2011; Cassar et al., 2015; Mendes et al, 2012; Mendes et al., 2018a). Microscopy may provide more precise taxonomic classification and additional ecological information through the observation of different life-cycle stages (such as the presence of resting cysts, auxospore formation or colonial vs. solitary forms), but is biased towards relatively large forms (> 5 µm) of phytoplankton groups with identifiable morphological characteristics, is time-consuming and needs a high level of expertise. In contrast, HPLC/CHEMTAX techniques can provide a comprehensive account of the main phytoplankton groups present in a sample, including those collected in oligotrophic areas (Roy et al., 2011). In the present work, we combined HPLC/CHEMTAX with microscopy observations of selected samples to obtain a robust and consistent view of the phytoplankton composition in the study zones. Comparisons between the two techniques must be interpreted with caution due to taxonomically and environmentally-related variability in biomarker pigments and Chl *a* content per biovolume, and to problems in biovolume estimates and in the microscopical identification of naked and small-celled groups (Kozlowski et al., 2011; Cassar et al., 2015). In this work, we found significant relationships between microscopy and chemotaxonomy for diatoms, autotrophic dinoflagellates and cryptophytes (Fig. S11). A strong correlation ($r^2 = 0.68$) was observed for diatoms, although there were some points, all belonging to the same station, for which the biovolume estimate was substantially lower than the CHEMTAX estimate, a discrepancy which could be attributed to sampling variability, errors in microscopy or overestimation by CHEMTAX due to contribution to Fuco from unidentified nanoplankton (Cassar et al., 2015). The correlation ($r^2 = 0.23$) was lower for autotrophic dinoflagellates, a finding that could be attributed to errors in the classification of auto- or heterotrophic forms and to the presence of peridinin-lacking species (Garibotti et al., 2003). The correlation coefficient ($r^2 = 0.68$) was relatively high for cryptophytes, but there was a disagreement between the two methods concerning their relative contribution to the phytoplankton community, especially at NSO (global average of 2% for microscopy vs 24% for CHEMTAX), an inconsistency which is likely to be caused by underestimation of the cryptophytes in the microscopic samples, as noted also by Rodríguez et al. (2002) and Cassar et al. (2015). A coarse check of those biovolume vs. Chl *a* relationships (ignoring intercept values) could be obtained from calculations of theoretical Chl *a* to biovolume ratios, which could be estimated using a standard C/Chl *a* ratio of 50 and the C to biovolume equations from Table 2 of Davies et al. (2016). For diatom and dinoflagellate cells between 5 and 40 µm of diameter this Chl *a*/biovolume value would span, respectively, from $2.6*10^{-6}$ to $0.8*10^{-6}$ (ng $\mu m^{-3}$) and from $7.1*10^{-6}$ to $2.3*10^{-6}$, fairly close to the slopes (Fig. S11) obtained from our field samples for diatoms ($6.4*10^{-7}$) and dinoflagellates ($1.35*10^{-6}$); however, the corresponding Chl *a*/biovolume ratios for cryptophytes ("Others") between 5 and 20 µm of diameter would be $3.3*10^{-6}$ to $2.6*10^{-6}$, well below the slope calculated for cryptophytes ($1.0*10^{-5}$), adding support to a possible underestimation of the latter by microscopy. The HPLC-CHEMTAX approach used in our study provided a comprehensive analysis of the phytoplankton composition and highlighted the importance of groups like cryptophytes, chlorophytes, haptophytes types 6 + 7, *Phaeocystis*-like, pelagophytes and prasinophytes in the global community (Figs. 5 and 6). Organisms of these groups tend to deteriorate easily in fixed samples and are difficult to identify by microscopy. In particular, cryptophytes were more important at NSO, SSO and WA than suggested by the microscopic observations, probably due to underestimation in the microscopic observations as discussed above, while most forms from the other groups that endured fixation became presumably pooled into nano- or microflagellate categories. The detection, in many samples, of *Phaeocystis*-like pigments by HPLC but not of *Phaeocystis* spp. cells by microscopy could be explained the presence of other haptophyte type 8 taxa or of non-colonial forms of *Phaeocystis* spp., which would have been counted as unidentified flagellates.

### 4.2. Ecophysiological hints from pigment composition

The mid-day decline of the ratio Fluo/Fl_Chl *a* (Fig. S3A) for the shallow samples is a common finding (Estrada et al., 1996; Mignot et al., 2011) and has been related to non-photochemical fluorescence quenching processes (Falkowski and Kolber, 1995; Sackmann et al., 2008), which in turn are influenced by factors such as community and pigment composition, and nutrient and light conditions. In our data set, the variability of the Fluo/Fl_Chl *a* ratio was particularly marked for SSO (Fig. S3A). This was the sub-region with lowest beam attenuation coefficients and the highest average $Z_{1\%}$/MLD relationship (Table 2), suggesting a higher potential for fluorescence quenching.

Consistent with the variation of specific fluorescence, the highest values of the ratio Ddx/LHC, indicative of the proportion of the photoprotective pigment Ddx with respect to the sum of the light-harvesting carotenoids 19-But, 19-Hex, Fuco and Per, were found throughout the shallow mixed layer of SSO (Fig. S6); at NSO, NSG and WA, the ratios were lower and started to decrease with depth within the upper part of the mixed layer, suggesting a faster time scale of photoacclimation relative to that of vertical mixing in the mixed layer of these sub-regions. The surface Ddx/LHC ratio (Figs. S6A and B) decreased with increasing MLD (Fig. S6D) and beam attenuation coefficient (data not shown), and was positively associated ($r^2 = 0.78$, N = 35, $p < 0.0001$) with $Z_{1\%}$ (Fig. 8A) in agreement with the expected enhancement of photoprotective pigment concentration with increased exposure to a relatively high irradiance environment (Goericke and Montoya, 1997; Cheah et al., 2017; Russo et al., 2018). Interestingly, the Chl *a*-normalized concentration of DMSP (DMSP/Fl_Chl *a*) exhibited the same pattern across zones as Ddx/LHC, i.e., it increased proportionally with light penetration as depicted by $Z_{1\%}$ ($r^2 = 0.70$, N = 34, $p < 0.0001$; Fig. 8B). DMSP is a cellular osmolyte

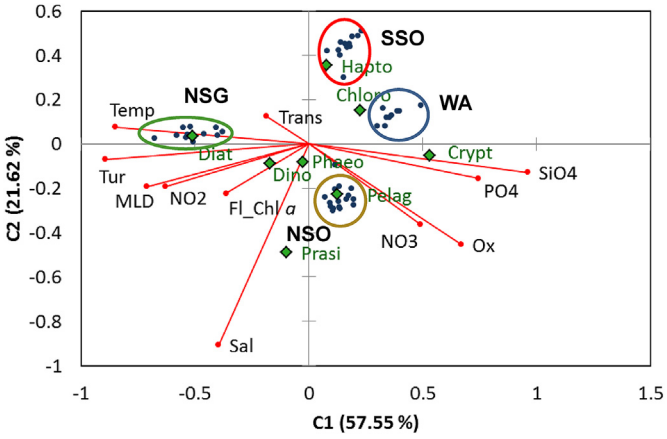


**Fig. 7.** Canonical correspondence analysis ordination plot of chemotaxonomic phytoplankton composition and abiotic parameters at surface (along with MLD). The first two axes explain 79.2% of the variance. Arrows indicate environmental variables [temperature (Temp), salinity (Sal), oxygen (Ox), turbidity (Tur), Transmission (Tr), nitrate (NO3), nitrite (NO2), silicate (SiO4), phosphate (PO4), mixed layer depth (MLD), Fl_Chl *a*]. Phytoplankton groups (diamonds) are chlorophytes (Chloro), cryptophytes (Crypt), diatoms (Diat), dinoflagellates (Dino), haptophytes 6+7 (Hapto), pelagophytes (Pelag), *Phaeocystis*-like (Phaeo), prasinophytes (Pras). Samples of the four sub-regions (circles) are encircled; See the explanation of Fig. 1 for acronyms.

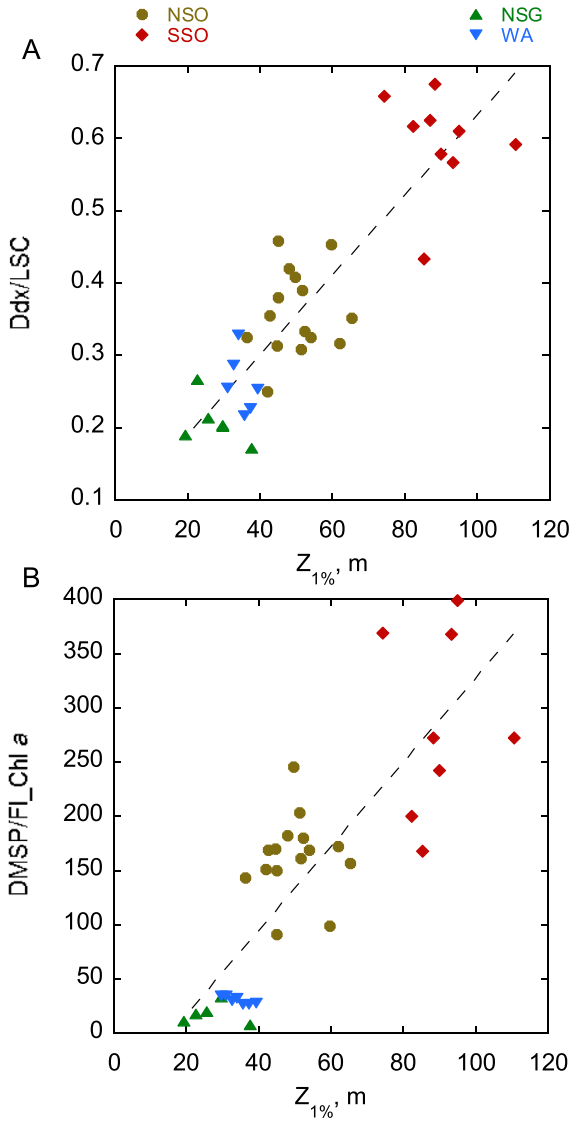


**Fig. 8.** Relationship of the euphotic zone depth ($z_{1\%}$, m) with the ratio Ddx/LHC (A) and the ratio DMSP/Fl_Chl *a* (B) for the study sub-regions. The equations are $y = 0.08 + 0.0055\times$, $r^2 = 0.78$, N = 35, $p < 0.0001$ (A) and $y = -60.35 + 3.88\times$, $r^2 = 0.70$, N = 34 (one outlier eliminated), $p < 0.0001$ (B). Acronyms as in Fig. 1.

mainly produced and harbored by phytoplankton, where it occurs at intracellular concentrations of up to hundreds of mM. Diatoms and cyanophytes typically are low DMSP producers, with DMSP/Chl *a* ratios between 0 and 4 nmol/μg, whereas haptophytes, dinoflagellates and chrysophytes are strong producers, with DMSP/Chl *a* ratios between 50 and > 100 nmol/μg (Stefels et al., 2007). Among other functions, DMSP is suggested to help microalgae cope with oxidative stress by producing reactive oxygen species scavengers (Sunda et al., 2002). Therefore, a combination of taxonomic composition and ecophysiological factors linked to environmental conditions appeared to underlie the distribution of phytoplankton DMSP content across the four sub-regions. While DMSP concentration did not correlate with any phytoplankton group, DMSP/Fl_Chl *a* was highest at SSO (Table 2), coinciding with a high proportion of haptophytes (CHEMTAX groups haptophytes types 6 + 7 and *Phaeocystis*-like) in the vicinity of sea ice (Stefels et al., 2018), the elevated exposure to solar radiation as depicted by the high values of the Ddx/LHC ratio, and presumably, also, iron limitation (Stefels et al., 2007). The lowest DMSP/Fl_Chl a ratio in NSG can be explained by the dominance of diatoms and a deeper, hence less illuminated, mixing layer (Bell et al., 2010; Galí and Simó, 2015).

### 4.3. Phytoplankton assemblages and environmental factors

The four zones visited in this study encompassed a wide spectrum of ecological characteristics. NSG was placed between the Polar Front and the Southern ACC Front (SACCF), in a region characterized by the regular occurrence of spring and summer phytoplankton blooms, fueled by the high concentrations of major nutrients and the availability of iron contributed by the ACC after its passage over the shelf waters around South Georgia (Korb et al., 2004; Whitehouse et al., 2008; Nielsdóttir et al., 2012). The relatively high temperatures in this region (mean ± SD, 4.73 °C ± 0.44) in comparison with other SO areas may also contribute to enhanced phytoplankton proliferation (Korb et al., 2004). The PEGASO stations were outside the main bloom area as seem from satellite imagery (Borrione and Schlitzer, 2013), but presented high Chl *a* concentrations (Tables 1 and 2, Figs. 3I and S2). Moderately lower nitrate and phosphate and much lower silicate concentrations at NSG than in the zones around the South Orkney Islands were consistent with a phytoplankton community dominated by well-silicified diatoms like *Eucampia antarctica*, *Thalassiosira* and *Porosira* spp. and *Odontella weissflogii*, typical of blooms in the area (Atkinson et al., 2001), complemented by substantial populations of haptophytes, including coccolithophores, and pelagophytes, as shown by our microscopy and HPLC-CHEMTAX analyses. However, at the time of our visit, the deep mixing layer of about 50 m compared with an average euphotic depth of 26 m (Table 2), and the relatively low silicate concentrations (average of 2 ± 0.4 μM at surface, Table 2) at the threshold for diatom dominance (Egge and Aksnes, 1992; Atkinson et al., 2001) were probably restricting phytoplankton growth.

The other three sub-regions visited in this study, with lower T_Chl *a* concentrations than NSG, presented macronutrient-replete conditions (Tables 1 and 2). Surface silicate concentrations exceeding 47 μM (Table 2), reflected a relatively low diatom contribution (Figs. 4 and 6). Lack of macronutrient depletion is typical of iron-limited regions of the SO (Venables and Moore, 2010). However, marine areas in the vicinity of islands and the West Antarctic Peninsula region may benefit from some benthic supply of iron from continental shelves (Nielsdóttir et al., 2012), a situation that can explain the relatively high Chl *a* concentrations in NSO and WA (Nielsdóttir et al., 2012; Murphy et al., 2013).

The main nano- and microplankton forms recorded by microscopy in NSO and SSO included the diatoms *Corethron pennatum* and *Fragilariopsis* spp., heterotrophic dinoflagellates like *Gyrodinium* spp. and *Protoperidinium* spp., unidentified autotrophic dinoflagellates, nanoflagellates and cryptophytes, all of which have been recorded in the region. Some differences, like the higher proportion of *Fragilariopsis* spp. in SSO could be attributed to the stronger sea ice influence (Cefarelli et al., 2010), which together with the lowest temperatures and Chl *a* concentrations can be taken as indicative of an earlier stage of phytoplankton bloom development in this zone. In transects across the Scotia Sea, from the vicinity of South Georgia to the South Orkney Islands, Korb et al. (2010) noted the abundance of *Corethron pennatum* and *Fragilariopsis* spp. and suggested that iron limitation could account for the high proportion of heterotrophic dinoflagellates, in agreement with our findings at SSO. On the other hand, some microscopy-based surveys in the South Orkney sub-region encountered a dominance of cryptophytes, prasinophytes and other nanoflagellates (Kopczyńska, 1991; Nielsdóttir et al., 2012). At WA, our CHEMTAX results highlighted the dominance of flagellates like cryptophytes and haptophytes 6 + 7, in agreement with the microscopic observations, which showed a high contribution of unidentified flagellates and cryptophytes, while diatoms were scarce. Several studies have shown the association of cryptophyte populations with shallow mixed layers influenced by ice melting (Schloss and Estrada, 1994; Mendes et al., 2018a, 2018b) and a shift from diatoms to cryptophytes has been described as characteristic

of the seasonal phytoplankton succession in the West Antarctic Peninsula region (Garibotti et al., 2003; Moline et al., 2004; Ducklow et al., 2007; Murphy et al., 2013; Mendes et al., 2018b). The gradient of increased T_Chl *a* concentrations and cryptophyte contribution from SSO to NSO and WA was associated with rising temperatures (Fig. S12), suggesting that it could be related, at least in part, to seasonal succession.

The position of the Chemtax groups in the space of the first axes of the CCA (Fig. 7) reflects in part the relationships discussed above, but it must be taken into account that relationships between biological and hydrographical variables may be the expression of the ecological history of a water body, rather than of direct effects. The association of diatoms with low nutrient concentrations reflects the consumption of major nutrients in the NSG sub-region, while the opposite situation of cryptophytes with respect to diatoms highlights their association to contrasting stages of phytoplankton succession. Other relationships in the graph, such as the association of haptophytes with low salinity and of prasinophytes with high salinity can also be interpreted in the context of a combination of ecological, successional and biogeographical factors.

An examination of the vertical distribution of the different phytoplankton categories reveals some consistent trends in the different study zones. Some groups, like haptophytes types 6 + 7 and *Phaeocystis*-like did not show marked vertical gradients within the euphotic zone. Cryptophytes, as noted above, tended to be more important in surface layers, while diatoms and pelagophytes increased their contribution at subsurface levels (Fig. 6). The ability of diatoms to thrive in relatively low light environments has been noted by a number of authors and has been attributed to features such as increased efficiency of ATP production (Fisher and Halsey, 2016). The increased abundance of pelagophytes in subsurface layers agrees with the observations of Latasa et al. (2017), who noted their preference for deeper levels within the deep chlorophyll maximum.

The average concentration of the biogenic trace gas DMS ranged 2–8 nM across sub-regions, being highest at NSO and SSO and lowest at WA (Table 2). DMS is produced from DMSP through the action of DMSP-lyases from phytoplankton and bacteria. The yield of the DMSP-to-DMS conversion is influenced by phytoplankton taxonomy and irradiance conditions, but also by ecological factors such as grazing-mediated mortality (Simó et al., 2018) or bacterial community composition and metabolism (Simó, 2004; Curson et al., 2011). The ratios DMS/DMSP and DMS/Fl_Chl *a* were highest in SSO, although the sea-ice marginal bloom was at the early phase of development, with expected low mortality rates. The likely explanation would be the coincidence of high irradiances with a large proportion of haptophytes, including *Phaeocystis*-like cells, which harbor high DMSP-lyase activity (Stefels et al., 2018). The lowest DMS/DMSP and DMS/Fl_Chl *a* ratios in WA are rather surprising, taking into account that the bloom there appeared to be in an advanced stage of development, as depicted by the abundance of protest grazers (data not shown); one reason might be the dominance of cryptophytes, which are poor DMS producers and have not been reported to harbor DMSP-lyases (Stefels et al., 2007).

## 5. Conclusion

As part of the PEGASO project, the main aims of this work were to characterize the ecophysiological variability of the phytoplankton in our study region and to ascertain the links between environmental properties and phytoplankton community structure. Microscopic observations and chemotaxonomic pigment analyses were used to ascertain the quantitative and qualitative composition of the phytoplankton in four contrasting sub-regions in the vicinity of South Georgia (NSG), the South Orkneys (NSO and SSO) and Anvers Islands (WA). Our findings confirmed previous observations such as the dominance of diatoms in the iron-rich South Georgia bloom sub-region, the overall importance of haptophytes and the association of cryptophytes with well-illuminated stratified surface waters influenced by ice melting, but also highlighted the substantial contribution of less well-studied forms such as the pelagophytes, important components of the picoplankton. The light stress condition of the phytoplankton community, an ecophysiological factor that is an important modulator of DMSP and DMS metabolism (Bell et al., 2010) was investigated by means of a photoprotective pigment index, which showed the highest values at SSO, the sub-region with the shallowest mixed layer and the deepest euphotic zone, and the lowest at NSG, where the mixed layer was deepest. The combination of light-adaptation, nutrient and taxonomy patterns regulated specific DMSP and DMS concentrations, with highly irradiated waters with high proportions of haptophytes being the most geared towards DMSP and DMS production.

## 6. Declarations of interest

None.

## Acknowledgements

The cruise was funded by the Spanish Ministry of Economy and Competitivity through project PEGASO (CTM2012-37615). S. N. was supported with a doctoral fellowship from the National Council of Technological and Scientific Development (CNPq) of Brazil. We thank Martí Galí for providing daily satellite imagery. We are grateful to the captain and crew of the BIO Hespérides, the technicians and researchers that participated in the cruise and the Unidad de Tecnología Marina (UTM) of the CSIC for their valuable help during the cruise. The authors thank Mara Abad for nutrient analyses and Carmen Cabeza for her great help with HPLC sample processing.

## Appendix A. Supplementary data

Supplementary data to this article can be found online at https://doi.org/10.1016/j.dsr.2019.06.005.

## References

Atkinson, A., Whitehouse, M.J., Priddle, J., Cripps, G.C., Ward, P., Brandon, M.A., 2001. South Georgia, Antarctica: a productive, cold water, pelagic ecosystem. Mar. Ecol. Prog. Ser. 216, 279–308.

Bell, T.G., Poulton, A.J., Malin, G., 2010. Strong linkages between dimethylsulphoniopropionate (DMSP) and phytoplankton community physiology in a large subtropical and tropical Atlantic Ocean data set. Glob. Biogeochem. Cycles 24, GB3009. http://doi:10.1029/2009GB003617.

Borrione, I., Schlitzer, R., 2013. Distribution and recurrence of phytoplankton blooms around South Georgia, Southern Ocean. Biogeosciences 10, 217–231.

Boyd, P.W., Trull, T.W., 2007. Understanding the export of biogenic particles in oceanic waters: is there consensus? Prog. Oceanogr. 72, 276–312.

Cassar, N., DiFiore, P.J., Barnett, B.A., Bender, M.L., Bowie, A.R., Tilbrook, B., Petrou, K., Westwood, K.J., Wright, S.W., Lefevre, D., 2011. The influence of iron and light on net community production in the Subantarctic and Polar Frontal Zones. Biogeosciences 8, 227–237.

Cassar, N., Wright, S.W., Thomson, P.G., Trull, T.W., Westwood, K.J., de Salas, M., Davidson, A., Pearce, I., Davies, D.M., Matear, R.J., 2015. The relation of mixed-layer net community production to phytoplankton community composition in the Southern Ocean. Glob. Biogeochem. Cycles 29, 446–462. http://doi:10.1002/2014GB004936.

Cefarelli, A.O., Ferrario, M.E., Almandoz, G.O., Atencio, A.G., Akselman, R., Vernet, M., 2010. Diversity of the diatom genus *Fragilariopsis* in the Argentine Sea and Antarctic waters: morphology, distribution and abundance. Polar Biol. 33, 1463.

Charlson, R.J., Lovelock, J.E., Andreae, M.O., Warren, S.G., 1987. Oceanic phytoplankton, atmospheric sulphur, cloud albedo, and climate. Nature 326, 655–661.

Cheah, W., Soppa, M.A., Wiegmann, S., Ossebaar, S., Laglera, L.M., Strass, V.H., Santos-Echeandía, J., Hoppema, M., Wolf-Gladrow, D., Bracher, A., 2017. Importance of deep mixing and silicic acid in regulating phytoplankton biomass and community in the iron-limited Antarctic Polar Front region in summer. Deep-Sea Res. II. 138, 74–85.

Chrétiennot-Dinet, M.J., 1990. Atlas du Fitoplancton Marin, vol. 3. Éditions du CNRS, Paris, France, pp. 261.

Cros, L., Fortuño, J.M., 2002. Atlas of northwestern mediterranean coccolithophores. Sci. Mar. 66 (Suppl. 1), 7–182.

Curson, R.J., Todd, J.D., Sullivan, M.D., Johnston, A.W.D., 2011. Catabolism of dimethylsulphoniopropionate: microorganisms, enzymes and genes. Nat. Rev. Microbiol. 9, 849–859.

Dall'Osto, M., Ovadnevaite, J., Paglione, M., Beddows, D.C.S., Ceburnis, D., Cree, C., Cortés, P., Zamanillo, M., Nunes, S.O., Pérez, G.L., Ortega-Retuerta, E., Emelianov, M., Vaqué, D., Marrasé, C., Estrada, M., Sala, M.M., Vidal, M., Fitzsimons, M.F., Beale, R., Airs, R., Rinaldi, M., Decesari, R., Facchini, M.C., Harrison, R.M., O'Dowd, C., Simó, R., 2017. Antarctic sea ice region as a source of biogenic organic nitrogen in aerosols. Sci. Rep. 7, 6047. https://doi.org/10.1038/s41598-017-06188-x.

Davies, C.H., Coughlan, A., Hallegraeff, G., Ajani, P., Armbrecht, L., Atkins, N., Bonham, P., Brett, S., Brinkman, R., Burford, M., Clementson, L., Coad, P., Coman, F., Davies, D., Dela-Cruz, J., Devlin, M., Edgar, S., Eriksen, R., Furnas, M., Hassler, C., Hill, D., Holmes, M., Ingleton, T., Jameson, I., Leterme, S.C., Lønborg, C., McLaughlin, J., McEnnulty, F., McKinnon, A.D., Miller, M., Murray, S., Nayar, S., Patten, R., Pausina, R.A., Pritchard, T., Proctor, R., Purcell-Meyerink, D., Raes, E., Rissik, D., Ruszczyk, J., Slotwinski, A., Swadling, K.M., Tattersall, K., Thompson, P., Thomson, P., Tonks, M., Trull, T.W., Uribe-Palomino, J., Waite, A.M., Yauwenas, R., Zammit, A., Richardson, A.J., 2016. A database of marine phytoplankton abundance, biomass and species composition in Australian waters. Scientific Data 3, 160043. http://doi:10.1038/sdata.2016.43, Accessed date: 11 April 2017.

Dinniman, M.S., Klinck, J.M., 2004. A model study of circulation and cross-shelf exchange on the west Antarctic Peninsula continental shelf. Deep-Sea Res. II. 51, 2003–2022.

Ducklow, H.W., Baker, K., Fraser, W.R., Martinson, D.G., Quetin, L.B., Ross, R.M., Smith, R.C., Stammerjohn, S., Vernet, M., 2007. Marine ecosystems: the West antarctic Peninsula. Phil. Trans. R. Soc. 362, 67–94.

Egge, J.K., Aksnes, D.L., 1992. Silicate as a regulating nutrient in phytoplankton competition. Mar. Ecol. Prog. Ser. 83, 281–289.

Estrada, M., Delgado, M., 1990. Summer phytoplankton distributions in the Weddell sea. Polar Biol. 10, 441–449.

Estrada, M., Marrasé, C., Salat, J., 1996. *In vivo* Fluorescence/chlorophyll *a* ratio as an ecological indicator in oceanography. Sci. Mar. 60, 317–325.

Falkowski, P.G., Kolber, Z., 1995. Variations in chlorophyll fluorescence yields in phytoplankton in the world oceans. Aust. J. Plant Physiol. 22, 341–355.

Fisher, N.L., Halsey, K.H., 2016. Mechanisms that increase the growth efficience of diatoms in low light. Photosynth. Res. 129, 183–197.

Frölicher, T.L., Sarmiento, J.L., Paynter, D.J., Dunne, J.P., Krasting, J.P., Winton, M., 2015. Dominance of the Southern Ocean in anthropogenic carbon and heat uptake in CMIP5 models. J. Clim. 28, 862–886.

Galí, M., Simó, R., 2015. A meta-analysis of oceanic DMS and DMSP cycling processes: disentangling the summer paradox. Glob. Biogeochem. Cycles 29. https://doi.org/10.1002/2014GB004940.

Garibotti, I.A., Vernet, M., Kozlowski, W.A., Ferrario, M.E., 2003. Composition and biomass of phytoplankton assemblages in coastal Antarctic waters: a comparison of chemotaxonomic and microscopic analyses. Mar. Ecol. Prog. Ser. 247, 27–42.

Garibotti, I.A., Vernet, M., Ferrario, M.E., 2005. Annually recurrent phytoplanktonic assemblages during summer in the seasonal ice zone west of the Antarctic Peninsula (Southern Ocean). Deep-Sea Res. I. 52, 1823–1841.

Gibberd, M.J., Kean, E., Barlow, R., Thomalla, S., Lucas, M., 2013. Phytoplankton chemotaxonomy in the Atlantic sector of the Southern Ocean during late summer 2009. Deep-Sea Res. I. 78, 70–78.

Goericke, R., Montoya, J.P., 1997. Estimating the contribution of microalgal taxa to chlorophyll *a* in the field-variations of pigment ratios under nutrient- and light-limited growth. Mar. Ecol. Prog. Ser. 169, 98–112.

Hansen, H.P., Koroleff, F., 1999. Determination of nutrients. In: Grasshoff, K., Kremling, K., Ehrhardt, M. (Eds.), Methods of Seawater Analyses. Wiley-VCH, Weinheim, pp. 161–228.

Higgins, H.W., Wright, S.W., Schlüter, L., 2011. Quantitative interpretation of chemotaxonomic pigment data, Phytoplankton Pigments. In: Roy, S., Llewellyn, C.A., Egeland, E.S., Johnsen, G. (Eds.), Characterization, Chemotaxonomy and Applications in Oceanography. Cambridge University Press, Cambridge, pp. 257–313.

Hillebrand, H., Dürselen, C.D., Kirschtel, D., Pollingher, U., Zohary, T., 1999. Biovolume calculation for benthic microalgae. J. Phycol. 35, 403–424.

Kopczyńska, E.E., 1991. Distribution of micro flagellates and diatoms in the sea-ice zone between elephant island and the south Orkney islands (december 1988 — january 1989). Pol. Polar Res. 12, 515–528.

Korb, R.E., Whitehouse, M., Ward, M., 2004. SeaWiFS in the southern ocean: spatial and temporal variability in phytoplankton biomass around South Georgia. Deep-Sea Res. II 51, 99–116.

Korb, R.E., Whitehouse, M.J., Gordon, M., Ward, P., Poulton, A.J., 2010. Summer microplankton community structure across the Scotia Sea: implications for biological carbon export. Biogeosciences 7, 343–356. www.biogeosciences.net/7/343/2010/.

Kozlowski, W.A., Deutschman, D., Garibotti, I., Trees, C., Vernet, M., 2011. An evaluation of the application of CHEMTAX to Antarctic coastal pigment data. Deep-Sea Res. I. 58, 350–364.

Latasa, M., 2007. Improving estimations of phytoplankton class abundances using CHEMTAX. Mar. Ecol. Prog. Ser. 329, 13–21.

Latasa, M., 2014. A simple method to increase sensitivity for RP-HPLC phytoplankton pigment analysis. Limnol Oceanogr. Methods 12, 46–53.

Latasa, M., Scharek, R., Vidal, M., Vila-Reixach, G., Gutiérrez-Rodríguez, A., Emelianov, M., Gasol, J.M., 2010. Preferences of phytoplankton groups for waters of different trophic status in the northwestern Mediterranean Sea. Mar. ecol. Prog. Ser. 407, 27–42.

Latasa, M., Cabello, A.M., Morán, X.A.G., Massana, R., Scharek, R., 2017. Distribution of phytoplankton groups within the deep chlorophyll maximum. Limnol. Oceanogr. 62, 665–685.

Luan, Q., Wang, C., Wang, X., Sun, J., Niu, M., Wang, J., 2013. Microphytoplankton communities off the Antarctic Peninsula region in austral summer 2010/2011. Pol. Polar Res. 34, 413–428.

Mackey, M.D., Mackey, D.J., Higgins, H.W., Wright, S.W., 1996. CHEMTAX - a program for estimating class abundances from chemical markers: application to HPLC measurements of phytoplankton. Mar. Ecol. Prog. Ser. 144, 265–283.

Marinov, I., Gnanadesikan, A., Sarmiento, J.L., Toggweiler, J.R., Follows, M., Mignone, B.K., 2008. Impact of oceanic circulation on biological carbon storage in the ocean and atmospheric pCO2. Glob. Biogeochem. Cycles 22, GB3007.

Martin, J., Fitzwater, S., Gordon, R., 1990. Iron deficiency limits phytoplankton growth in antarctic waters. Glob. Biogeochem. Cycles 4, 5–12.

Mendes, C.R.B., de Souza, M.S., Tavano, V.M., Leal, M.C., Brotas, V., Garcia, C.A.E., 2012. Dynamics of phytoplankton communities during late summer around the tip of the Antarctic Peninsula. Deep-Sea Res. I. 65, 1–14.

Mendes, C.R.B., Tavano, V.M., Leal, M.C., Souza, M.S., Brotas, V., Garcia, C.A.E., 2013. Polar Biol. vol. 36. pp. 537–547. http://10.1007/s00300-012-1282-4.

Mendes, C.R.B., Kerr, R., Tavano, V.M., Cavalheiro, F.A., Garcia, C.A.E., Dessai, D.R.G., Anilkumar, N., 2015. Cross-front phytoplankton pigments and chemotaxonomic groups in the Indian sector of the Southern Ocean. Deep-Sea Res. II. 118, 221–232.

Mendes, C.R.B., Tavano, V.M., Kerr, R., Dotto, T.S., Maximiano, T., Secchi, E.R., 2018a. Impact of sea ice on the structure of phytoplankton communities in the northern Antarctic Peninsula. Deep-Sea Res. II. 149, 111–123. http://doi.org/10.1016/j.dsr2.2017.12.003.

Mendes, C.R.B., Tavano, V.M., Dotto, T.S., Souza, M.S., Kerr, R., Garcia, C.A.E., Secchi, E.R., 2018b. New insights on the dominance of cryptophytes in Antarctic coastal waters: a case study in Gerlache Strait. Deep-Sea Res. II. 149, 161–170. https://doi.org/10.1016/j.dsr2.2017.02.010.

Meredith, M.P., Nicholls, K.W., Renfre, I.A., Boehme, L., Biuw, M., Fedak, M., 2011. Seasonal evolution of the upper-ocean adjacent to the south Orkney islands, Southern Ocean: results from a "lazy biological mooring". Deep-Sea Res. II. 58, 1569–1579.

Mignot, A., Claustre, H., D'Ortenzio, F., Xing, X., Poteau, A., Ras, J., 2011. From the shape of the vertical profile of in vivo fluorescence to Chlorophyll-a concentration. Biogeosciences 8, 2391–2406.

Moline, M.A., Prézelin, B.B., Schofield, O., 1997. Palmer-LTER: stable inter-annual successional patterns of phytoplankton communities in the coastal waters off Palmer Station, Antarctica. Antarctic Journal 151–153.

Moline, M.A., Claustre, H., Frazer, T.K., Schofield, O., Vernet, M., 2004. Alteration of the food web along the Antarctic Peninsula in response to a regional warming trend. Glob. Chang. Biol. 10, 1973–1980.

Monterey, G., Levitus, S., 1997. Seasonal Variability of Mixed Layer Depth for the World Ocean. NOAA Atlas NESDIS 14, vol. 96. U.S. Gov. Printing Office, Washimgton D.C., pp. 87.

Moore, C.M., Mills, M.M., Arrigo, K.R., Berman-Frank, I., Bopp, L., Boyd, P., Galbraith, W., E. D, Geider, R.J., Guieu, C., Jaccard, S.L., Jickells, T.D., La Roche, J., Lenton, T.M., Mahowald, N.M., Marañón, E., Marinov, I., Moore, J.K., Nakatsuka, T., Oschlies, A., Saito, M.A., Thingstad, T.F., Tsuda, A., Ulloa, O., 2013. Processes and patterns of oceanic nutrient limitation. Nat. Geosci. 6, 701–710.

Murphy, E.J., Hofmann, E.E., Watkins, J.L., Johnston, N.M., Piñones, A., Ballerini, T., Hill, S.L., Trathan, P.N., Tarling, G.A., Cavanagh, R.A., Young, E.F., Thorpe, S.E., Fretwell, P., 2013. Comparison of the structure and function of Southern Ocean regional ecosystems: the antarctic Peninsula and South Georgia. J. Mar. Syst. 109–110, 22–42.

Nielsdóttir, M.C., Bibby, T.S., Moore, C.M., Hinz, D.J., Sanders, R., Whitehouse, M., Korb, R., Achterberg, E.P., 2012. Seasonal and spatial dynamics of iron availability in the Scotia Sea. Mar. Chem. 130–131, 62–72.

Orsi, A.H., Whitworth III, T.W., Nowlin Jr., W.D., 1995. On the meridional extent and fronts of the Antarctic Circumpolar Current. Deep-Sea Res. Part I. 42, 641–673.

Priddle, J., Heywood, R.B., Theriot, E., 1986. Some environmental factors influencing phytoplankton in the Southern Ocean around South Georgia. Polar Biol. 5, 65–79.

Rampi, L., Bernard, M., 1980. Chiave per la determinazione delle peridinee pelagiche mediterranee. Comitato Nazionale Energia Nucleare- RT/BIO, Roma, Italy, pp. 193 (80)8.

Ricard, M., 1987. Diatomophycées. Atlas du Fitoplancton Marin, vol. 2. Éditions du CNRS, Paris, France, pp. 297.

Rodríguez, F., Varela, M., Zapata, M., 2002. Phytoplankton assemblages in the Gerlache and Bransfield Straits (Antarctic Peninsula) determined by light microscopy and CHEMTAX analysis of HPLC pigment data. Deep-Sea Res. II. 49, 723–747.

Roy, S., Llewellyn, C.A., Egeland, E.S., Johnsen, G., 2011. Phytoplankton Pigments: Characterization, Chemotaxonomy and Applications in Oceanography. Cambridge University Press, Cambridge.

Russo, A.D.P.G., de Souza, M.S., Mendes, C.R.B., Jesus, B., Tavano, V.M., Garcia, C.A.E., 2018. Spatial variability of photophysiology and primary production rates of the phytoplankton communities across the western Antarctic Peninsula in late summer 2013. Deep-Sea Res. II. 149, 99–110. https://doi.org/10.1016/j.dsr2.2017.09.021.

Sackmann, B.S., Perry, M.J., M.J., Eriksen, C.C., 2008. Seaglider observations of variability in daytime fluorescence quenching of chlorophyll-a in Northeastern Pacific coastal waters. Biogeosci. Discuss. 5, 2839–2865.

Schlitzer, R., 2016. Ocean Data view. http://odv.awi.de.

Schloss, I., Estrada, M., 1994. Phytoplankton composition in the Weddell-Scotia confluence area during austral spring in relation to hydrography. Polar Biol. 14, 77–90.

Simó, R., 2001. Production of atmospheric sulfur by oceanic plankton: biogeochemical, ecological and evolutionary links. Trends Ecol. Evol. 16, 287–294.

Simó, R., 2004. From cells to globe: approaching the dynamics of DMS(P) in the ocean at multiple scales. Can. J. Fish. Aquat. Sci. 61, 673–684.

Simó, R., Saló, V., Almeda, R., Movilla, J., Trepat, I., Saiz, E., Calbet, A., 2018. The quantitative role of microzooplankton grazing in dimethylsulfide (DMS) production in the NW Mediterranean. Biogeochemistry 141, 125–142.

Sournia, A., 1986. Atlas du Fitoplancton Marin, vol. 1. Editions du CNRS, Paris, France, pp. 219.

Stefels, J., Steinke, M., Turner, S., Malin, G., Belviso, S., 2007. Environmental constraints

on the production and removal of the climatically active gas dimethylsulphide (DMS) and implications for ecosystem modelling. Biogeochemistry 83, 245–275.
Stefels, J., van Leeuwe, M.A., Jones, E.M., Meredith, M.P., Venables, H.J., Webb, A.L., Henley, S.F., 2018. Impact of sea-ice melt on dimethyl sulfide (sulfoniopropionate) inventories in surface waters of Marguerite Bay, West Antarctic Peninsula. Phil. Trans. R. Soc. A 376, 20170169. https://doi.org/10.1098/rsta.2017.0169.
Sunda, W., Kieber, D.J., Kiene, R.P., Huntsman, S., 2002. An antioxidant function for DMSP and DMS in marine algae. Nature 418, 317–320.
Tomas, C.R., 1993. Marine Phytoplankton. A Guide to Naked Flagellates and Coccolithophorids. Academic Press, San Diego, USA, pp. 263.
Tomas, C.R., 1995. Identifying Marine Diatoms and Dinoflagellates. Academic Press, San Diego, USA, pp. 598.
UNESCO, 1995. Manual on harmful marine microalgae (Tech. Editor) In: Hallegraeff, G.M., Anderson, D.M., Cembella, A.D., Enevoldsen, H.O. (Eds.), Intergovernmental Oceanographic Commission, Manuals and Guides N°33, Paris, France, pp. 551.
Utermöhl, H., 1958. Zur Vervolkommung der quantitativen Phytoplankton-methodik. Mitt. Int. Ver. Theor. Angew. Limnol. 9, 1–38.
Venables, H., Moore, C.M., 2010. Phytoplankton and light limitation in the Southern Ocean: learning from high-nutrient, high-chlorophyll areas. J. Geophys. Res. 115, C02015.
Vernet, M., Martinson, D., Iannuzzi, R., Stammerjohn, S., Kozlowski, W., Sines, K., Smith, R., Garibotti, I., 2008. Primary production within the sea-ice zone west of the Antarctic Peninsula: I — sea ice, summer mixed layer, and irradiance. Deep-Sea Res. II. 5, 2068–2085.
Ward, P., Meredith, M.P., Whitehouse, M.J., Rothery, P., 2008. The summertime plankton community at South Georgia (Southern Ocean): comparing the historical (1926/1927) and modern (post 1995) records. Prog. Oceanogr. 78, 241–256.
Whitehouse, M.J., Korb, R.E., Atkinson, A., Thorpe, S.E., Gordon, M., 2008. Formation, transport and decay of an intense phytoplankton bloom within the High-Nutrient Low-Chlorophyll belt of the Southern Ocean. J. Mar. Syst. 70, 150–167.
Yentsch, C.S., Menzel, D.W., 1963. A method for the determination of phytoplankton chlorophyll and phaeophytin by fluorescence. Deep-sea Res. 10, 221–231.